

CERN-EP-2026-042
17 February 2026

Inclusive $\psi(2S)$ production at midrapidity in pp collisions at $\sqrt{s} = 13$ TeV

ALICE Collaboration*

Abstract

Inclusive production of $\psi(2S)$ mesons is measured for the first time at midrapidity ($|y| < 0.9$) in pp collisions at $\sqrt{s} = 13$ TeV using the ALICE detector at the LHC. The measurement is performed in the transverse-momentum (p_T) range of 4 to 16 GeV/c and is based on events triggered by the Transition Radiation Detector, corresponding to an integrated luminosity of $1.7 \pm 1.8\%$ (syst.) pb^{-1} . The p_T -differential production cross section of the $\psi(2S)$ and its ratio to the J/ψ production cross section are presented. The results extend the accessible p_T range down to 4 GeV/c, and a mild rise of the $\psi(2S)$ -to- J/ψ cross section ratio with increasing p_T is observed. The measurements are compared with theoretical predictions based on NRQCD and the ICEM model.

arXiv:2602.22848v1 [hep-ex] 26 Feb 2026

© 2026 CERN for the benefit of the ALICE Collaboration.

Reproduction of this article or parts of it is allowed as specified in the CC-BY-4.0 license.

*See Appendix A for the list of collaboration members

1 Introduction

Charmonia, such as J/ψ or $\psi(2S)$, are bound states of a valence charm and anti-charm quark. Charmonia can be produced directly in the hadronic interaction, from decays of higher-mass charmonium states, or from weak decays of beauty hadrons. The first two contributions are referred to as prompt production, while the latter corresponds to non-prompt production. At low transverse momenta, direct production dominates, while beyond transverse momenta of 10 GeV/c, non-prompt production from decays of beauty hadrons becomes comparable to the direct component [1, 2].

The prompt production is governed by different scales, in particular the hard scale of the charm-quark mass and the soft scales of the charm-quark momenta in the charmonium rest frame and the charmonium binding energy [3]. Because of these very different scales, theoretical calculations assume that the hard production of the $c\bar{c}$ pair and the soft hadronization process factorize [4]. In this ansatz, one separates the short-distance perturbative hard scattering process from the long-distance non-perturbative dynamics, which are encoded in long-distance matrix elements (LDMEs). The dominant process for the production of a $c\bar{c}$ pair at LHC energies is gluon fusion. The LDMEs, obtained from global fits to a wide range of quarkonium production and polarization measurements, are commonly assumed to be universal. However, recent studies of open heavy-flavor fragmentation suggest that universality in heavy-flavor hadronization, i.e. independence of the collision system and energy, does not hold: the ALICE Collaboration observed significantly enhanced production of charmed baryons compared to results from electron–positron and electron–proton collisions [5], and a similar enhancement was recently reported by the LHCb Collaboration in the beauty sector [6]. While fragmentation fractions and LDMEs describe different aspects of non-perturbative dynamics, these findings highlight that heavy-flavor hadronization can depend on the collision environment. Comparatively, much less is known experimentally about hadronization of charm-quark pairs into quarkonia.

Different treatments of the non-perturbative processes have led to various theoretical models of charmonium formation. Shortly after the discovery of the J/ψ , the Color Singlet Model (CSM) [7–11] was introduced. Under the assumption that the $c\bar{c}$ pair evolving into the quarkonium state is in a color-singlet state (CS), the production of on-shell heavy-quark pairs with the same quantum numbers as the quarkonium state is modeled using perturbative Quantum Chromo Dynamics (pQCD). The production rates are determined by the CS $c\bar{c}$ wave functions and their derivatives and can be related to quarkonium decay rates. While successful at low energies, this model significantly underestimates the observed production cross section, even using calculations at next-to-leading order (NLO) in the strong coupling constant α_s [12] at the Tevatron and LHC energies [13, 14]. The Non-Relativistic Quantum ChromoDynamics framework (NRQCD)[15] extends the CSM by including contributions from heavy-quark pairs produced in a color-octet (CO) state, in addition to the CS contributions. The transition probability from the CO $c\bar{c}$ state to a CS charmonium state is expanded in powers of the relative velocity between the heavy quarks and parameterized using LDMEs. These LDMEs are free parameters fitted to experimental data. Recently, NLO extensions of NRQCD [16–18] have successfully described quarkonium production cross sections for many different collision systems and energies. At the same time, they struggle to account for the measured polarization at intermediate and high p_T from the CDF Collaboration at the Tevatron, while ALICE data at the LHC at intermediate p_T are well reproduced [19–22].

The Color Evaporation Model (CEM) [23–25] is based on the concept of quark-hadron duality. It is assumed that the heavy-quark pair evolves into a quarkonium state when the invariant mass is below the production threshold corresponding to twice the mass of the lightest open heavy-flavor meson. The probability of the quark pair to evolve into a specific quarkonium state is determined by one proportionality factor that is assumed to be universal. Once the factor is fixed, transverse-momentum and rapidity (y) distributions of the quarkonium can be predicted without additional free parameters. Consequently, the ratio between the yields of two quarkonium states formed from a given heavy-quark pair is expected to be independent of collision energy, p_T , and y . The Improved Color Evaporation Model (ICEM) [26]

employs the k_T -factorization approach, which introduces a p_T dependence due to the p_T of incoming gluons and off-shell properties. As in the CEM, the transition probability to a bound charmonium state is proportional to the $c\bar{c}$ pair production cross section integrated over an invariant-mass range from the mass of the bound state to twice the mass of the lightest D meson.

Measurements of production rates of different charmonium states in proton–proton (pp) collisions at the LHC are interesting to test the various production mechanisms. In particular, they provide a testing ground for the concepts of factorization and universal fragmentation. Measurements of bottomonium production at the CDF and at the LHC experiments indicated different populations from excited states [27, 28]. This suggests that similar variations may arise in charmonium production because charmonium states are more sensitive to higher-order QCD corrections [29] and to medium effects in heavy-ion collisions [30]. The charmonium measurements in pp collisions also provide a baseline for proton-nucleus and nucleus–nucleus results, where charmonia are prominent observables to study the quark–gluon plasma [31].

In this paper, we report results on the inclusive p_T -differential production cross sections of $\psi(2S)$ at midrapidity ($|y| < 0.9$) and the $\psi(2S)$ -to- J/ψ cross section ratio measured in pp collisions at $\sqrt{s} = 13$ TeV for the first time. While the inclusive J/ψ production cross section in pp collisions has previously been published using minimum-bias (MB) triggered data [32], the ratio presented here is obtained consistently within the present analysis. This was made possible by using a level-1 trigger of the Transition Radiation Detector (TRD) to enhance the sampled luminosity.

These results complement the measurement at forward rapidity by the ALICE Collaboration [2] and extend the p_T range to lower value compared with midrapidity measurements by the CMS Collaboration for $p_T > 20$ GeV/c [33] and by the ATLAS Collaboration for $p_T > 8$ GeV/c [34]. Measurements of the $\psi(2S)$ production cross section in pp collisions at midrapidity were already performed by the CMS and ATLAS Collaborations for $p_T > 6.5$ GeV/c and $p_T > 10$ GeV/c, respectively, but at lower collision energies, as reported in Refs. [35–37].

In the following, the ALICE detector, the trigger setup, and the data sample are described in Section 2. The data analysis and the determination of systematic uncertainties are detailed in Section 3. The results are presented and discussed in the context of recent model calculations in Section 4, and the summary is given in Section 5.

2 Experimental setup, data sample, and event selection

This section focuses on the detectors used for reconstructing the J/ψ and $\psi(2S)$ at midrapidity. A comprehensive description of the ALICE detector and its performance can be found in Refs. [38, 39].

Electron and positron tracks from J/ψ and $\psi(2S)$ decays are reconstructed as global tracks using the Inner Tracking System (ITS) [40] and the Time Projection Chamber (TPC) [41], which cover the full azimuthal angle and the pseudorapidity interval $|\eta| < 0.9$. These detectors are placed within a solenoid magnet providing a uniform magnetic field of $B = 0.5$ T parallel to the beam direction. The ITS is composed of six layers of detectors. From the innermost to the outermost layers, it includes two layers each of silicon pixel, drift, and strip detectors, allowing for precise reconstruction of primary and secondary vertices. The Silicon Pixel Detector (SPD) layers, are placed at radial distances of 3.9 and 7.6 cm from the nominal Interaction Point (IP) and are used for reconstructing the primary vertex, providing crucial information for track reconstruction. The TPC is a cylindrical gas drift detector located at radial distances between 85 and 250 cm from the IP and covers ± 250 cm from the IP along the beam direction. It provides particle-identification (PID) information through the measurement of specific ionisation energy loss (dE/dx), as well as up to 159 space points for reconstructing charged-particle tracks. The Transition Radiation Detector (TRD) [42] consists of 522 drift chambers arranged in six concentric layers at radial

distances between 2.90 and 3.68 m from the IP, in five stacks along the longitudinal direction, covering the pseudorapidity interval $|\eta| < 0.84$. Each chamber contains a foam/fibre sandwich radiator, followed by a drift region and a multiwire proportional chamber (MWPC) with an amplification and readout section, both filled with a Xe-CO₂ gas mixture. The TRD provides three-dimensional position information, used to reconstruct short local track segments (tracklets) in each chamber. These tracklets are then used for track reconstruction and for electron identification through the measured charge deposition and, in particular, through transition radiation. The V0 counters [43], two arrays of 32 scintillator tiles each, have a pseudorapidity coverage of $2.8 < \eta < 5.1$ (V0A) and $-3.7 < \eta < -1.7$ (V0C) and provide trigger and event-selection information.

The data used in this analysis have been recorded with the TRD trigger by the ALICE Collaboration during the LHC Run 2 data-taking campaigns of 2017 and 2018 for pp collisions at $\sqrt{s} = 13$ TeV. A MB data sample, triggered by the coincidence of signals in the V0A and V0C detectors and collected during the same campaign, is used to estimate the TRD-trigger efficiency. Events are required to have a reconstructed vertex located within $|z_{\text{vtx}}| < 10$ cm from the IP along the beam direction. The SPD and V0 detectors are used to reject background from beam-gas interactions and pile-up events using algorithms that identify multiple vertices, as described in Ref. [39]. The remaining fraction of pile-up events is negligible.

For these campaigns, a TRD trigger at level 1, about 6 μs after the collision was introduced to trigger on electrons and positrons of intermediate and high p_T . A single-electron trigger with a p_T threshold of 2 GeV/c and likelihood selections based on the TRD signal was employed to increase the probability of selecting events containing quarkonia decays. This trigger configuration substantially enhances the recorded yields of inclusive J/ψ and $\psi(2S)$ candidates compared with the MB trigger. An enhancement factor is defined as the ratio of the number of reconstructed electron candidates per event in the TRD-triggered sample to that in the MB sample. This factor is approximately 34 for the present pp dataset at $\sqrt{s} = 13$ TeV, illustrating the enrichment of electron-containing events provided by the TRD trigger. Additional track quality criteria are imposed, requiring five tracklets (reconstructed in individual TRD layers) per stack, including a tracklet in the first layer, and a minimum value for the TRD track sagitta ($\Delta p_T^{-1} < 0.2$ c/GeV) of the TRD track to reduce background from photon conversions in the detector material before the TRD. For more details on the use of the TRD trigger for J/ψ measurements, see Ref. [44].

The total number of events after selection (N_{TRD}) is 1.78×10^8 , corresponding to an integrated luminosity of $1.7 \text{ pb}^{-1} \pm 1.8\%$ (syst.). The integrated luminosity was evaluated separately for each year based on the MB trigger cross section determined from van der Meer scans [45], as described in Ref. [46].

3 Data analysis

Inclusive J/ψ and $\psi(2S)$ meson production is measured using TRD-triggered events, similar to the measurement of J/ψ production in p-Pb collisions in ALICE [44]. Both J/ψ and $\psi(2S)$ mesons are reconstructed via the dielectron decay channels, with branching ratios (BR) of $5.971 \pm 0.032\%$ and $0.794 \pm 0.022\%$ for J/ψ and $\psi(2S)$, respectively [47]. Due to the trigger condition requiring a single electron with transverse momentum of $p_T \geq 2$ GeV/c, the acceptance and efficiency for J/ψ and $\psi(2S)$ mesons are limited to $p_T > 2$ GeV/c.

The p_T -differential production cross section is obtained by correcting the raw number of reconstructed charmonium candidates, N_{ψ}^{raw} , for the acceptance and efficiency ($A \times \epsilon$) in the corresponding p_T and y intervals. The definitions and evaluations of these correction terms are described in Section 3.3. The full expression for the p_T -differential cross section, including the normalisation to the branching ratio, integrated luminosity, and the widths of the p_T and rapidity intervals, is given by

$$\frac{d^2\sigma}{dydp_T} = \frac{N_{\psi}^{\text{raw}}}{(A \times \varepsilon) \times \text{BR} \times \Delta p_T \times \Delta y \times \mathcal{L}_{\text{int}}}. \quad (1)$$

Here, \mathcal{L}_{int} is the integrated luminosity of the TRD-triggered data sample given by $\mathcal{L}_{\text{int}} = N_{\text{MB}}/\sigma_{\text{MB}}$, where σ_{MB} is the MB trigger cross section [46]. The number of equivalent MB events, N_{MB} , is determined as $N_{\text{MB}} = N_{\text{TRD}} \times f_{\text{norm}}$, where the number of TRD-triggered events, N_{TRD} , is scaled with a normalisation factor, f_{norm} , evaluated for each run. This factor accounts for the enhancement due to the trigger selection and represents the inverse of the probability for a MB event to also satisfy the TRD-trigger condition. The weighted average value of f_{norm} across the dataset is approximately 570.

The efficiencies are determined through Monte Carlo (MC) simulations. Minimum-bias pp events are generated with PYTHIA 6.4 using the Perugia 2011 tune [48], and one J/ψ and one $\psi(2S)$ meson are embedded in each event. Prompt J/ψ and $\psi(2S)$ are injected with flat rapidity distributions. The p_T distribution of the J/ψ is reweighted to match a measurement at midrapidity at $\sqrt{s} = 13$ TeV [32]. For the $\psi(2S)$, the measurement at forward rapidity at $\sqrt{s} = 13$ TeV [2] is used up to 6 GeV/c, and a flat distribution is assumed at higher p_T . The p_T distributions are then iteratively reweighted following Ref. [2]. In each iteration, the acceptance times efficiency correction is updated using the corrected p_T -differential cross section, and the procedure is repeated until the difference between the input and output corrected spectra is below about 1%. Both prompt J/ψ and $\psi(2S)$ are assumed to be unpolarised. In addition, non-prompt J/ψ and $\psi(2S)$ are generated from the decays of beauty hadrons using the PYTHIA generator. Their decays to charmonia are simulated using the EvtGen package [49], which provides a proper description of beauty-hadron decay channels as well as radiative charmonium decays. All generated particles are transported through the ALICE detector modeled using GEANT3 [50].

To reproduce the TRD-trigger condition as in the data, the simulation includes an emulation of the TRD online trigger logic, applying the electron and positron likelihood estimated from TRD and track segment requirements used during data taking. The TRD-trigger efficiency for electrons or positrons ($\varepsilon_{\text{TRD}}(p_T^e)$)¹ is defined as

$$\varepsilon_{\text{TRD}}(p_T^e) = \frac{N_e^{\text{TRD, MB}}(p_T^e)}{N_e^{\text{MB}}(p_T^e)}, \quad (2)$$

where N_e^{MB} is the number of reconstructed single-electron (or positron) tracks identified in MB data using the TPC, and $N_e^{\text{TRD, MB}}$ is the number of those tracks that are also selected by the TRD trigger.

The TRD-trigger efficiency for electrons and positrons exhibits time-dependent variations due to changes in the magnetic field and the gas mixture, which affect the detector gain. Therefore, the TRD-trigger efficiency is determined by accounting for run-wise dependencies of the magnetic field and gas conditions. This is done by evaluating the efficiency for each run and computing a weighted average using the corresponding fraction of TRD-triggered events [44]. The p_T dependence of the TRD-trigger efficiency is parametrized with a fit, and the MC simulation is tuned to reproduce the fitted efficiency.

Figure 1 shows the TRD-trigger efficiency for electrons (left) and positrons (right) as a function of the reconstructed p_T of the global track. The p_T threshold is clearly visible by the rapid increase in efficiency at 2 GeV/c, followed by a plateau at higher p_T . The plateau value for electrons is slightly higher than the one for positrons and has a sharper turn-on curve. Below 2 GeV/c, non-zero values for the TRD-trigger efficiency for electrons and positrons are found. These non-zero values arise from the presence of high- p_T electrons or positrons in the same event that satisfy the online TRD-trigger condition, rather than the low- p_T tracks themselves. This contribution is referred to as the underlying-event effect in the following. An error function is employed to fit the TRD-trigger efficiency, shown as a red line, with an offset accounting for the underlying-event effect. A softer rise of the trigger efficiency above

¹It should be noted that $\varepsilon_{\text{TRD}}(p_T^e)$ represents the single-track trigger efficiency, whereas $\varepsilon_{\text{TRDtrg}}$ discussed later in Section 3.3 denotes the efficiency for a charmonium candidate to pass the trigger requirement via any of its decay electrons.

2 GeV/c is observed for positrons, which is attributed to the $E \times B$ effect. This effect originates from the perpendicular orientation of the electric and magnetic fields in the drift region of the TRD chambers, which causes drifting electrons to follow a direction aligned with negative tracks and rotated with respect to positive tracks [42]. As a consequence, the performance of track-segment reconstruction and the likelihood calculation differs for electrons and positrons.

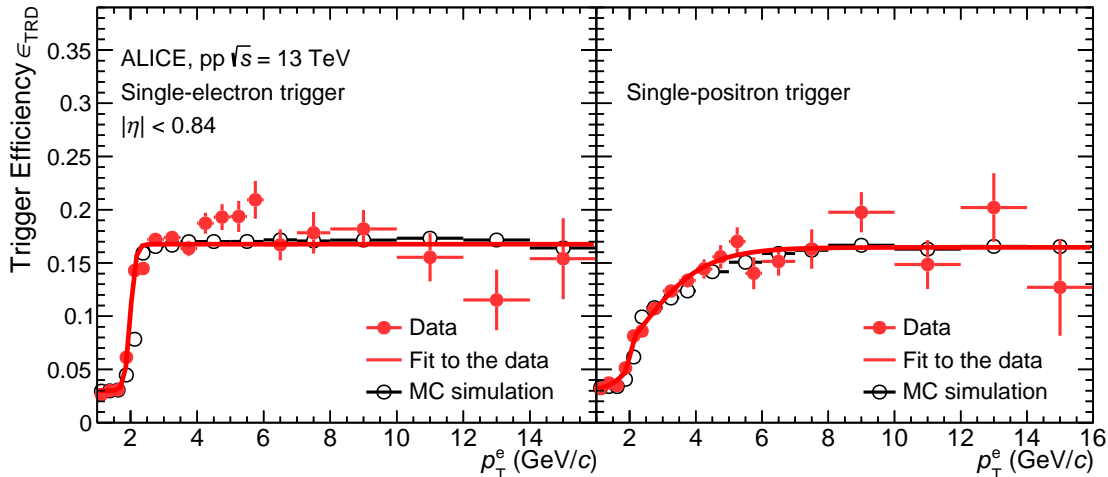


Figure 1: Acceptance times TRD-trigger efficiency ($\epsilon_{\text{TRD}}(p_T^e)$) described by Eq. 2 for single electrons (left) and positrons (right) obtained from TRD-triggered data (red solid circle), fitted with an error function (red line), and MC simulation (black open circle). See text for details.

3.1 Track selection

Tracks are required to have at least 70 out of 159 clusters in the TPC and hits in at least 2 of the 6 ITS layers. A hit in the innermost layer of the SPD is specifically required to suppress background electrons from photon conversions in the detector material. Tracks are selected within the TRD kinematic acceptance, with p_T larger than 1 GeV/c and pseudorapidity $|\eta| < 0.84$. To further suppress background electrons and tracks originating from weak decays, tracks with a Distance-of-Closest-Approach (DCA) to the primary vertex larger than 0.2 cm in the transverse plane and 0.4 cm along the beam axis are rejected. The transverse DCA resolution is better than 75 μm for charged particles with $p_T > 1$ GeV/c [51]. Additionally, to reduce contributions from photon conversions, any track forming an opposite-sign pair with invariant mass below 0.05 GeV/c² is excluded. This selection is verified with MC simulations to have a negligible impact on the charmonium signal.

Good quality tracks are identified as electrons (and positrons) based on their dE/dx measured in the TPC. Specifically, the variable n_{σ_i} is used. It represents the deviation (in units of standard deviations) of the measured energy loss from the expected value for a given particle hypothesis i . Electron candidates are required to satisfy $-2 < n_{\sigma_e} < 3$. To reject contamination from proton and charged pion (π), tracks with momenta $p < 5$ GeV/c and $|n_{\sigma_{p,\pi}}| < 3$ are vetoed. For tracks with momenta $p > 5$ GeV/c, a looser criterion of $|n_{\sigma_{p,\pi}}| < 2$ is applied to improve the reconstruction efficiency and retain a sufficient number of electron candidates.

3.2 Signal extraction

The raw yields of J/ψ and $\psi(2S)$ in each p_T interval are obtained from the invariant-mass distributions of opposite-sign (OS) electron–positron pairs (m_{ee}) formed within the same event (SE). These distributions contain contributions from the signal (J/ψ and $\psi(2S)$) as well as background. The dominant background consists of electron–positron pairs from uncorrelated processes, mostly semi-leptonic heavy-flavor decays combined with light vector meson decays.

This uncorrelated combinatorial background is estimated using the mixed-event (ME) technique, as employed in previous measurements [32, 52]. To construct the ME background, each event is assigned to a mixing pool defined by a similar number of SPD tracklets (short track segments reconstructed in the two layers of the SPD) and a similar primary vertex position (z -vertex). Mixing is performed using events within the same run, corresponding to a stable data-taking period. The OS distribution from mixed events is normalised using the ratio of the same-event like-sign to mixed-event like-sign distributions in the mass range $2 < m_{ee} < 4 \text{ GeV}/c^2$, where contributions from correlated sources are expected to be small.

After subtracting the uncorrelated background using the ME technique, the remaining distribution is fitted using signal templates of J/ψ and $\psi(2S)$ obtained from the MC simulation described in the previous section. A second-order polynomial function is used to describe the residual background mostly coming from correlated electron pairs from semi-leptonic decays of heavy-flavor hadrons [53]. The raw number of J/ψ and $\psi(2S)$ is obtained by integrating the signal distributions in the invariant-mass intervals $2.92 < m_{ee} < 3.16 \text{ GeV}/c^2$ and $3.52 < m_{ee} < 3.76 \text{ GeV}/c^2$, respectively. The quality of the fit, expressed as the χ^2/NDF , ranged from 1.21 to 1.10 across the considered p_T intervals, decreasing from low to high electron–positron pair p_T (p_T^{ee}).

Figure 2 shows the invariant-mass distributions of electron–positron pairs for the lowest (left) and highest (right) p_T^{ee} intervals. These distributions include contributions from signal (J/ψ and $\psi(2S)$), correlated background (primarily from heavy-flavor decays), and uncorrelated combinatorial background estimated with the ME technique. The uncorrelated background is shown as the gray area. Although the signal extraction fit is performed after subtracting this ME background, the ME component is added back and overlaid in the figure for illustrative purposes. The total fit function is decomposed into the correlated background (blue shaded area) and the signal peaks (red). Even in the lowest dielectron pair- p_T interval ($4 < p_T^{ee} < 6 \text{ GeV}/c$), the invariant-mass distribution displays a visible $\psi(2S)$ peak with a statistical significance of 3.9σ . This constitutes the first measurement of $\psi(2S)$ at midrapidity at the LHC at such low p_T . The significance of the $\psi(2S)$ signal is improved by the larger integrated luminosity available at low p_T compared to the MB data and by the improved electron selection due to the TRD online PID. The lower p_T reach is constrained by the signal-to-background ratio rather than by the kinematic threshold imposed by the trigger requirements.

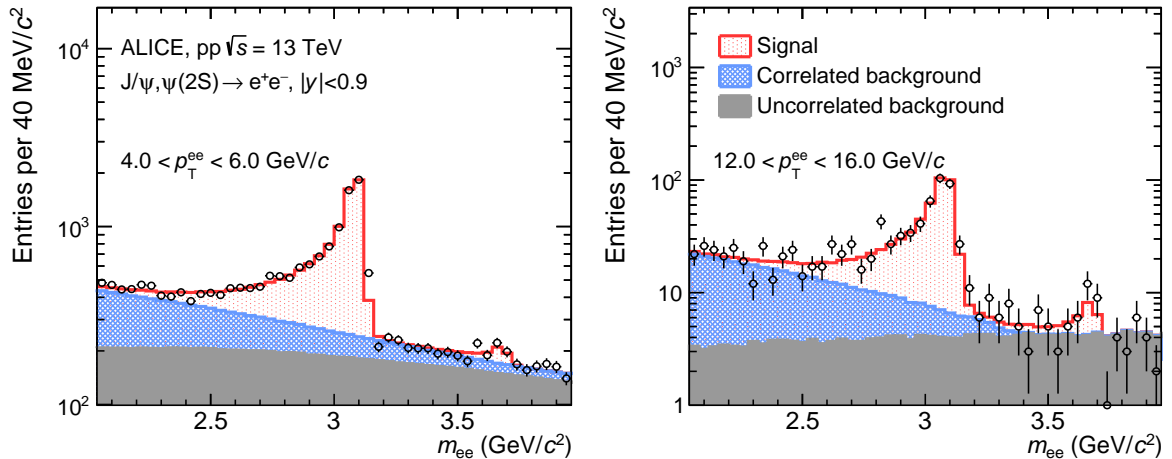


Figure 2: Invariant-mass distributions of e^+e^- pairs in the same event for the lowest (left) and the highest (right) p_T^{ee} intervals. Superimposed to the data are the fits containing the signals of J/ψ and $\psi(2S)$ and the correlated (blue area) and uncorrelated (gray area) background sources (see text).

3.3 Corrections

The corrections for acceptance and efficiency ($A \times \varepsilon$) are obtained from MC simulations and include the product of the following components: (i) the kinematic acceptance (A); (ii) the reconstruction efficiency ($\varepsilon_{\text{reco}}$), which accounts for both tracking and PID efficiencies; (iii) the efficiency due to the finite integration mass window used for extracting the J/ψ and $\psi(2S)$ yields ($\varepsilon_{\text{mass}}$); and (iv) the TRD-trigger efficiency ($\varepsilon_{\text{TRDtrg}}$), which represents the probability that an event containing a charmonium decay satisfies the TRD-trigger condition. The acceptance and total efficiency, with its individual contributions, are shown in Fig. 3 for J/ψ (left) and $\psi(2S)$ (right).

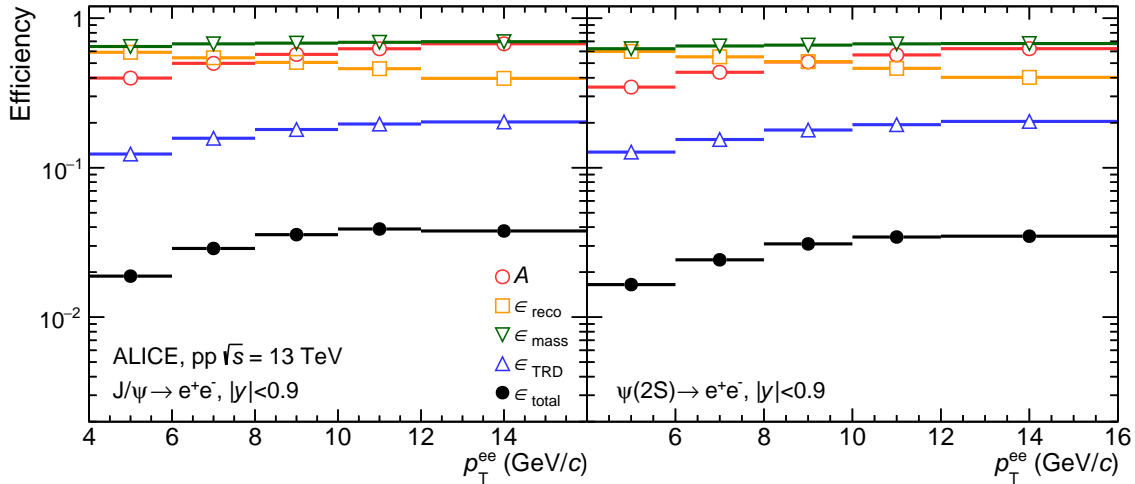


Figure 3: Acceptance and efficiency as a function of p_T^{ee} for inclusive J/ψ (left) and $\psi(2S)$ (right). In addition to the total efficiency, its individual contributions are shown.

The TRD-trigger efficiency of J/ψ and $\psi(2S)$ is emulated in MC simulations by implementing the same online trigger algorithm as described above. To evaluate the TRD-trigger efficiency of charmonia, only events containing prompt J/ψ and $\psi(2S)$ are used to avoid an artificial enhancement of the trigger probability from additional electrons produced in beauty-hadron decays. In addition, the efficiency is also evaluated by selecting only those candidates for which the trigger is fired by one of their own decay electrons. In the simulations, both charmonia are embedded in the same event and forced to decay into dielectrons, which increases the number of lepton pairs compared to real data and consequently raises the likelihood that at least one track fulfills the TRD-trigger condition. This contribution is found to be independent of p_T . The underlying-event contribution included in $\varepsilon_{\text{TRDtrg}}$ is therefore also taken into account in the charmonium trigger efficiency.

3.4 Systematic uncertainties

Table 1 summarizes the sources of systematic uncertainty for the p_T -differential cross section measurements of J/ψ , $\psi(2S)$, and the $\psi(2S)$ -to- J/ψ ratio. In order to obtain stable estimates and minimize the impact of statistical fluctuations, the uncertainties are evaluated in two broader p_T intervals: 4–8 and 8–16 GeV/c . These intervals are selected based on the similarity of background shapes and signal-to-background ratios (S/B). The uncertainties are evaluated by varying the specific criteria relevant to each source and calculating the root mean square of the resulting distributions. The total systematic uncertainty used for the cross section is calculated as the quadratic sum of all individual sources, excluding contributions from the branching ratios and integrated luminosity.

The systematic uncertainty of the tracking efficiency is determined as the quadratic sum of the uncertainties from the ITS–TPC matching efficiency and from the efficiency of the track-quality selections. The uncertainty of the ITS–TPC matching efficiency is derived from residual differences between data and

Table 1: Summary of systematic uncertainties for the J/ψ and $\psi(2S)$ yields, and the $\psi(2S)$ -to- J/ψ yield ratio, evaluated in the p_T intervals 4–8 and 8–16 GeV/c .

p_T (GeV/c)	J/ψ		$\psi(2S)$		$\psi(2S)/J/\psi$	
	4–8	8–16	4–8	8–16	4–8	8–16
Tracking	5.4%	7.1%	5.4%	7.1%	cancels	
PID	1.2%	3.4%	1.2%	3.4%	cancels	
Signal extraction	1.9%	1.9%	3.3%	2.9%	3.8%	4.4%
Fit	1.6%	1.8%	9.9%	9.2%	10.0%	9.4%
MC p_T shape	2.8%		2.0%		3.4%	
TRD-trigger efficiency	5.0%		5.0%		cancels	
Branching ratio	0.54%[47]		2.8%[47]		2.9%	
Luminosity			1.8%[46]		cancels	

MC simulations for single-track matching, as described in Ref. [54]. Since this uncertainty is found to be independent of the particle species, it is propagated to dielectron pairs from J/ψ and $\psi(2S)$ decays, yielding values between 4% and 5% depending on p_T . The uncertainty of the track quality is obtained by varying the corresponding selection criteria.

The systematic uncertainty on PID is determined by varying the PID selection criteria. Both the electron-identification cuts and the hadron-rejection criteria are varied in data and MC simulations.

For $\psi(2S)$, the same tracking and PID systematic uncertainties as for J/ψ are assigned. This approach reduces the impact of statistical fluctuations in the uncertainty estimation. To validate this assumption, the reconstruction efficiencies (including tracking and PID) for electrons from J/ψ and $\psi(2S)$ decays are compared. The ratio of the efficiencies is found to be constant for $p_T > 2 \text{ GeV}/c$, indicating similar detector response and selection efficiency in this p_T region. Therefore, assigning the same tracking and PID systematic uncertainties to both charmonium states is justified. Consequently, these uncertainties cancel in the $\psi(2S)$ -to- J/ψ ratio.

The systematic uncertainty related to the signal extraction is determined by varying the limits of the invariant-mass interval of the e^+e^- pair for signal integration. This is done by extending or reducing the integration interval by $40 \text{ MeV}/c^2$ to $80 \text{ MeV}/c^2$ in upper and lower direction. The data are corrected for the fraction of signal outside of the integration interval.

The systematic uncertainty related to the invariant-mass fit is determined by varying the functions corresponding to the correlated background and signal shape and the fit range. Even in the high- p_T region, the S/B for $\psi(2S)$ is around 2, indicating that the background contribution remains non-negligible, and the background fit still contributes significantly to the overall uncertainty.

The initial p_T distributions of J/ψ and $\psi(2S)$ used in the MC simulations are reweighted to match measurements of the J/ψ at midrapidity and of the $\psi(2S)$ at forward rapidity [2, 32]. The systematic uncertainty associated with the input p_T distributions is evaluated by varying these spectra and propagating the effect to the acceptance and efficiency corrections. As alternative input shapes, the J/ψ p_T distribution measured at forward rapidity [2] is used for J/ψ , while the midrapidity J/ψ distribution scaled according to the m_T -scaling prescription [2, 55] is used for $\psi(2S)$.

The systematic uncertainty on the TRD-trigger efficiency for J/ψ and $\psi(2S)$ is obtained by varying the likelihood threshold used in the trigger decision within the integer granularity of the front-end electronics, following the procedure described in Ref. [44]. This uncertainty accounts for possible residual differences between data and simulation in the TRD PID response due to imperfect modelling of detector conditions, such as pressure and gas composition. In addition, in the determination of the TRD-trigger efficiency for electrons (Eq. 2), both correlated and uncorrelated electron contributions are included. In dielectron decays from charmonia, the trigger decision can be fired by either the electron or the positron

in the pair. Consequently, an electron that does not directly satisfy the trigger requirement may still appear in a triggered event due to its correlated partner. This effect leads to a slight p_T -dependent enhancement of the estimated efficiency, increasing the absolute trigger efficiency by up to about one percentage point in the simulation. Since correlated and uncorrelated contributions cannot be disentangled in real data, this variation is introduced to conservatively cover the associated uncertainty and any residual differences between data and simulation.

The uncertainty of the integrated luminosity includes contributions from the beam luminosity estimated via a van der Meer scan (1.8%) [46] and from the TRD trigger normalisation factor (0.2%). These two components are added in quadrature and cancel in the $\psi(2S)$ -to- J/ψ ratio. The uncertainty of the branching ratios to the dielectron channels is taken from Ref. [47].

4 Results

4.1 p_T -differential production cross section

In Fig. 4, the p_T -differential inclusive $\psi(2S)$ production cross section measured by ALICE is compared with results from the ATLAS Collaboration [34], covering p_T ranges of $8 < p_T < 140$ GeV/c ($|y| < 0.75$). For the ALICE data, statistical and systematic uncertainties are represented by error bars and boxes, respectively. The uncertainties on branching ratios of $\psi(2S)$ to electrons and muons of about 2.8% and 7.5%, respectively, are not included in the boxes. In order to account for the non-linearity of the steeply falling spectrum within each p_T interval, the ALICE data points in the figure are placed at the interval-averaged p_T value following the Lafferty-Wyatt prescription [56]. To enable a direct comparison to the inclusive ALICE measurements, the ATLAS data points are obtained by summing the prompt and non-prompt cross sections reported in Ref. [34]. In this procedure, the uncertainties of the prompt and non-prompt components are assumed to be correlated when forming the inclusive uncertainty. The statistical and systematic uncertainties of the resulting inclusive points are then added in quadrature and shown as error bars for visual clarity. The integrated luminosity uncertainty is now shown in the figure; it amounts to 1.8% for ALICE and to 1.13% ($p_T < 60$ GeV/c) and 0.83% ($p_T \geq 60$ GeV/c) for ATLAS [34].

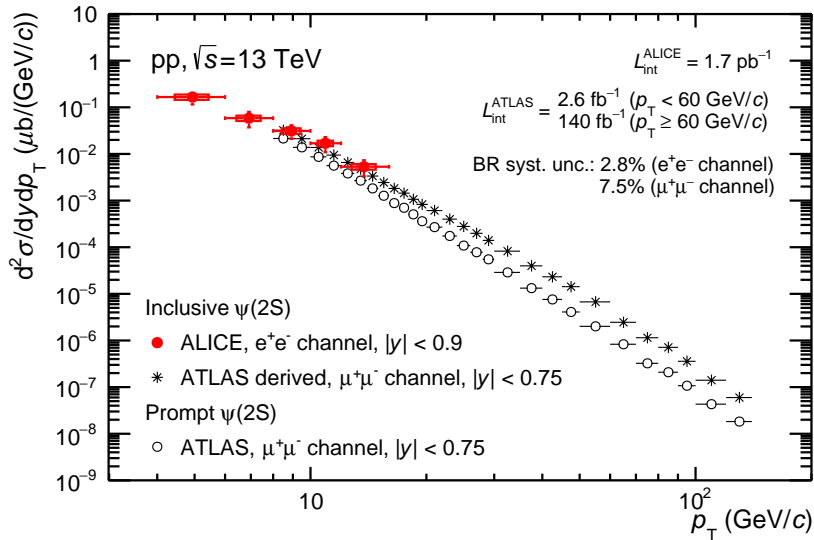


Figure 4: p_T -differential inclusive $\psi(2S)$ production cross section at midrapidity in pp collisions at $\sqrt{s} = 13$ TeV. Statistical and systematic uncertainties are shown as error bars and boxes, respectively, and data points are plotted according to the Lafferty–Wyatt prescription [56]. The data points for the inclusive production are obtained by summing the published prompt and non-prompt measurements [34]. The statistical and systematic uncertainties are combined in quadrature. Uncertainties related to integrated luminosity are not shown.

In the overlapping p_T region, the inclusive $\psi(2S)$ production cross section is fully consistent with the derived ATLAS data in the range 8–16 GeV/c within the uncertainties. The ALICE measurement extends the accessible p_T range from 8 down to 4 GeV/c.

In Fig. 5, the inclusive p_T -differential $\psi(2S)$ production cross section in pp collisions at $\sqrt{s} = 13$ TeV at midrapidity ($|y| < 0.9$) is shown and fitted with a power-law function

$$f(p_T) = K \times \frac{p_T}{(1 + (p_T/p_0)^2)^n}, \quad (3)$$

with K , p_0 , and n as free parameters. The fit describes the data well, with $\chi^2/\text{NDF} = 0.45$.

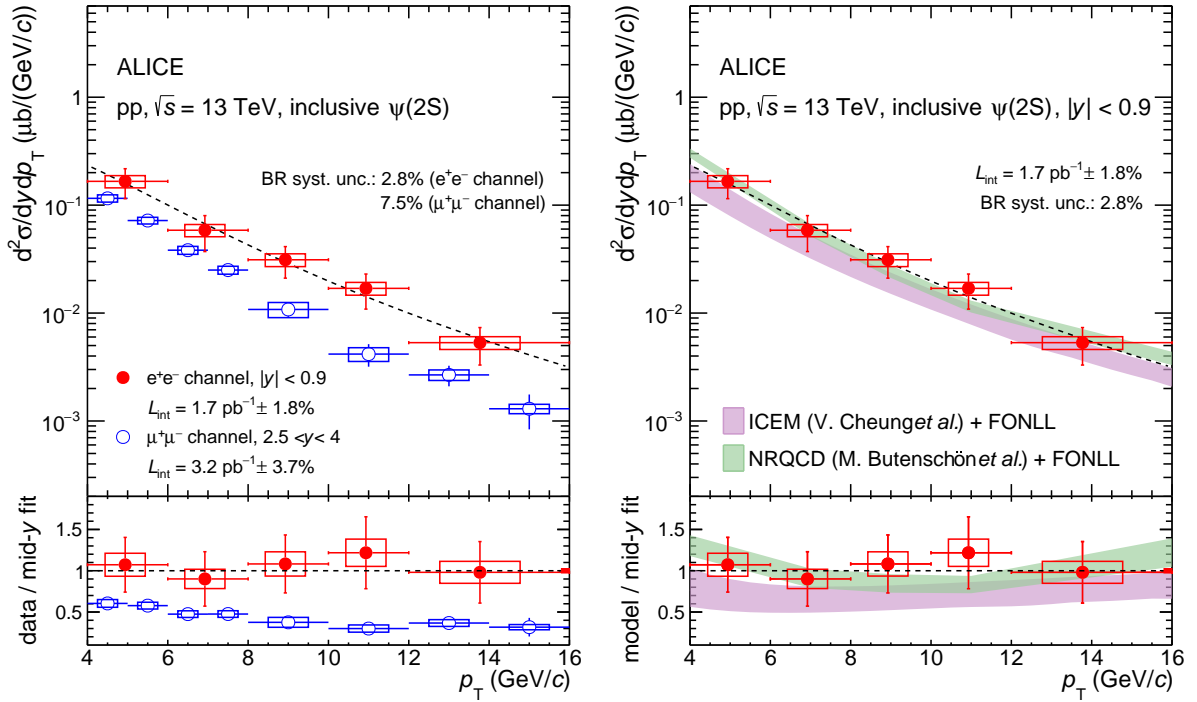


Figure 5: p_T -differential inclusive $\psi(2S)$ production cross section at midrapidity in pp collisions at $\sqrt{s} = 13$ TeV is compared with ALICE results at forward rapidity [2] (left) and with the model calculations from ICEM [57] and NRQCD [3] (right). Both calculations include a non-prompt contribution from beauty-hadron decays via FONLL [58]. Data points are plotted according to the Lafferty–Wyatt prescription [56]. The lower panels show the ratios of the data points or model calculations to the power-law fit to the midrapidity data.

The comparison of J/ψ production between mid and forward rapidity was studied in Ref. [32] and showed a hardening of the p_T spectrum at midrapidity compared to forward rapidity. The corresponding comparison for $\psi(2S)$ is presented in this paper. In the left panel of Fig. 5, the $\psi(2S)$ production cross section at midrapidity is compared to the measurement at forward rapidity [2]. The lower panel shows the ratios of the $\psi(2S)$ measurements at midrapidity and forward rapidity to the power-law fit to the midrapidity data. The uncertainty boxes in the lower panel represent the quadratic sum of the systematic uncertainties of the data points and the uncertainty of the fit-function mean in the given p_T interval. The ratio of the measurements at forward rapidity to the fit to the midrapidity results decreases by about a factor of two between 4.5 and 15 GeV/c, indicating a harder $\psi(2S)$ spectrum at midrapidity compared to forward rapidity. This is consistent with the behavior observed for the J/ψ spectra [32].

In the right panel of Fig. 5, the p_T -differential inclusive $\psi(2S)$ production cross section is compared with results from two model calculations, the ICEM [57] model and NRQCD [3]. Both calculations only include prompt $\psi(2S)$ production; therefore, a non-prompt $\psi(2S)$ component due to weak decays

of b hadrons is added to these model calculations, obtained by using the Fixed-Order Next-to-Leading-Logarithms (FONLL) approach by Cacciari et al. from Ref. [58]. The non-prompt fraction, defined as the ratio of non-prompt to inclusive $\psi(2S)$ production, increases from 10% at low p_T to 49% at $p_T = 16$ GeV/c.

The lower panel of the right-hand side of the figure shows again the ratios to the power-law fit to the $\psi(2S)$ data. The bands represent the uncertainties of the model calculations. These uncertainties mostly arise from variations in the renormalisation and factorization scales and the charm-quark mass. The NLO NRQCD calculation by Butenschoen et al. in Ref. [3] employs the factorization formalism, where the production cross section is decomposed into short-distance coefficients, calculated perturbatively, and LDMEs. These are fitted to experimental data and account for contributions from various intermediate Fock states. They are assumed to be universal. In contrast, the ICEM by Cheung et al. from Ref. [57] uses the k_T -factorization approach and includes a single normalisation parameter to account for long-distance effects [59] instead of using LDMEs.

The NRQCD results have a small uncertainty and are in agreement with the experimental data over the full p_T range, similar to observations made already at forward rapidity [2]. The ICEM predictions are also consistent with the data within uncertainties, although the calculation tends to lie near the lower edge of the measured cross sections. This behaviour is mainly due to the harder p_T spectrum predicted by the model and the fitting procedure used to determine the overall normalisation, which is strongly influenced by low- p_T CDF data [60].

4.2 $\psi(2S)$ -to- J/ψ cross section ratio

Figure 6 shows the inclusive $\psi(2S)$ -to- J/ψ cross section ratio measured by the ALICE Collaboration in pp collisions at $\sqrt{s} = 13$ TeV, compared with results from ATLAS [34]. The J/ψ cross section used in the ratio is obtained from the present analysis and is verified to be fully consistent with previous ALICE measurements [2]. The statistical and systematic uncertainties of the ALICE results are represented by error bars and boxes, respectively. The luminosity uncertainty cancels out in the ratio, and the uncertainties due to the branching ratios are shown in the legend. Inclusive $\psi(2S)$ -to- J/ψ data (solid black circles) from the ATLAS Collaboration are reconstructed by first summing the published prompt and non-prompt components of each state to obtain their inclusive cross sections [34], and then taking their ratio. The statistical and systematic uncertainties of the two components are treated as uncorrelated and combined in quadrature. The inclusive $\psi(2S)$ -to- J/ψ production cross section ratio measured by ALICE is consistent with the corresponding result from ATLAS [34].

In the left panel of Fig. 7, the p_T -differential $\psi(2S)$ -to- J/ψ cross section ratio is compared with measurements at forward rapidity in pp collisions at the same center-of-mass energy [2]. The two measurements are compatible within current uncertainties, indicating no significant rapidity dependence in the $\psi(2S)$ -to- J/ψ cross section ratio. A mild increase of the inclusive $\psi(2S)$ -to- J/ψ cross section ratio as a function of p_T is observed in both cases, although the uncertainties are large, especially at high p_T . The observed trend may be partially due to feed-down contributions from higher mass states such as $\psi(2S)$ and χ_c .

In the right panel of Fig. 7, the inclusive $\psi(2S)$ -to- J/ψ cross section ratio is compared with model calculations. The uncertainties of theoretical calculations from variations of scales and masses cancel out in the ratio. Theory bands are obtained by taking the ratio of the upper and lower bounds of $\psi(2S)$ and J/ψ model calculations. In models like ICEM, J/ψ from feed-down from higher charmonium states has softer p_T spectra than their parent particles, leading to a slightly rising ratio with increasing p_T . In contrast, NRQCD predicts genuinely harder p_T spectra for heavier states, reflecting hard scattering kinematics. The observed trend may result from a combination of small higher-state feed-down effects and intrinsic production dynamics. The NRQCD model shows good agreement within the relatively large model uncertainties over the entire measured p_T range, consistent with observations at forward rapidity [2]. The size of the uncertainty of the NRQCD calculation on the $\psi(2S)$ -to- J/ψ cross section

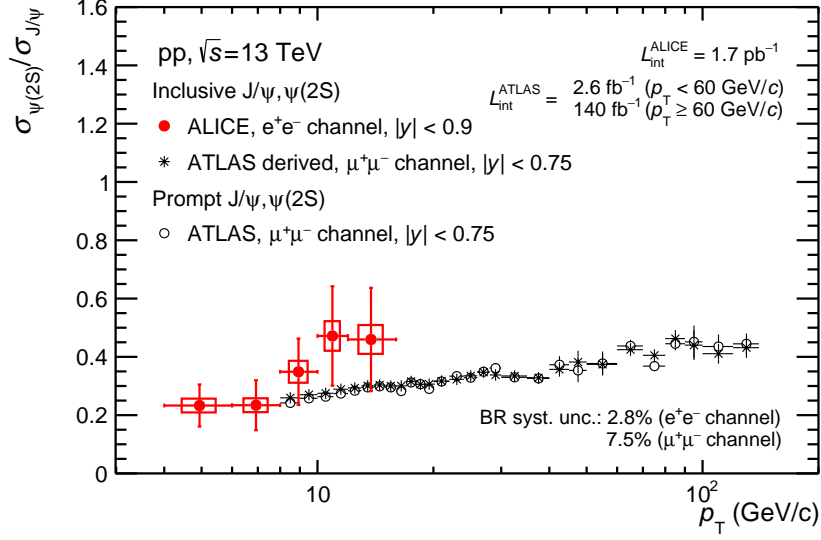


Figure 6: p_T -differential $\psi(2S)$ -to- J/ψ production cross section ratio measured by the ALICE and the ATLAS Collaborations at midrapidity in pp collisions at $\sqrt{s} = 13$ TeV [34]. For the ALICE Collaboration, statistical and systematic uncertainties are shown as error bars and boxes, respectively, and data points are plotted according to the Lafferty–Wyatt prescription [56]. Inclusive $\psi(2S)$ -to- J/ψ points from the ATLAS Collaboration (solid black circles) are obtained by summing the published prompt and non-prompt components of each state [34], and taking their ratio. Statistical and systematic uncertainties are treated as uncorrelated and combined in quadrature.

ratio arises from the LDMEs fits, which start at low p_T and include a large number of datasets. The ICEM calculation describes the J/ψ cross section within uncertainties in the $4 < p_T < 16$ GeV/ c range [2], while underestimating the $\psi(2S)$ yield. Since ICEM assumes a p_T dependence of prompt charmonium production independent of collision energy and rapidity, it inherently predicts an almost flat $\psi(2S)$ -to- J/ψ ratio, whereas the data show an increasing trend with p_T .

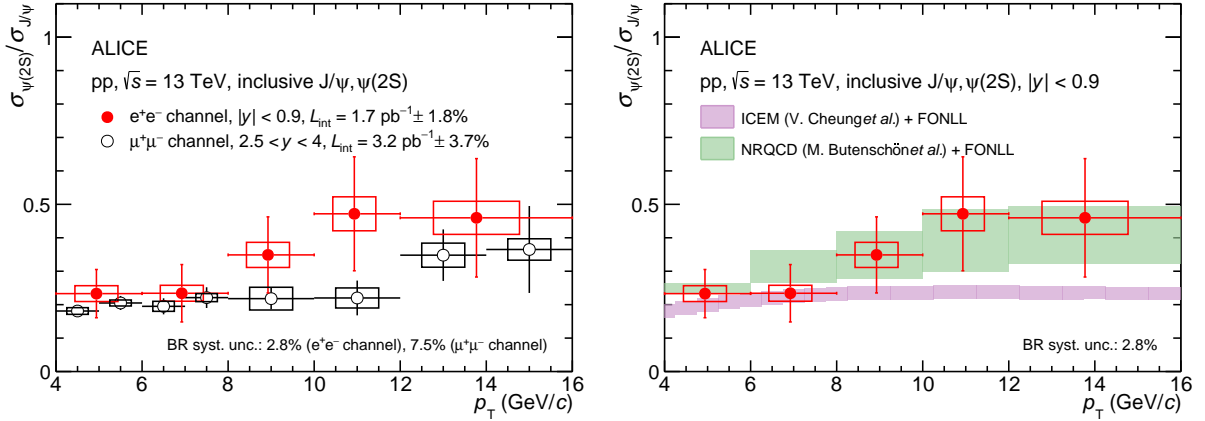


Figure 7: p_T -differential $\psi(2S)$ -to- J/ψ production cross section ratio at midrapidity in pp collisions at $\sqrt{s} = 13$ TeV compared with a measurement at forward rapidity in pp collisions at the same collision energy [2] (left), and compared with the model calculations [3, 57, 58] (right). The error bars indicate the statistical uncertainties, and the boxes indicate the systematic uncertainties. The data points are plotted at the effective p_T values evaluated according to the Lafferty–Wyatt prescription [56]. The widths of the bands reflect the theoretical uncertainties.

5 Summary

The inclusive p_T -differential production cross section of $\psi(2S)$ mesons and the ratio to the J/ψ cross section have been measured at midrapidity ($|y| < 0.9$) in pp collisions at $\sqrt{s} = 13$ TeV for the first time with the ALICE detector at the LHC. The measurements are reported for the p_T range of 4 to 16 GeV/ c using data collected with the online single-electron trigger from the Transition Radiation Detector. This analysis extends the accessible rapidity and p_T ranges compared to previous studies at the LHC, providing new insights into charmonium production at relatively low p_T . Comparison with theoretical predictions shows that NRQCD calculations describe the data quantitatively over the entire measured p_T range. A mild rise in the $\psi(2S)$ -to- J/ψ cross section ratio with increasing p_T is observed, consistent within uncertainties with the trend predicted by NRQCD. While the ICEM results are also consistent within errors with the measured $\psi(2S)$ spectrum, the ratio of $\psi(2S)$ -to- J/ψ shows a significantly weaker increase with p_T , which is inherent to the ICEM approach. The ALICE results of the $\psi(2S)$ cross section and the $\psi(2S)$ -to- J/ψ cross section ratio are consistent with the inclusive measurements derived from ATLAS results in the overlapping p_T region and extend the coverage from 8 GeV/ c down to 4 GeV/ c , a region not accessible in other experiments.

Acknowledgements

The ALICE Collaboration would like to thank all its engineers and technicians for their invaluable contributions to the construction of the experiment and the CERN accelerator teams for the outstanding performance of the LHC complex. The ALICE Collaboration gratefully acknowledges the resources and support provided by all Grid centres and the Worldwide LHC Computing Grid (WLCG) collaboration. The ALICE Collaboration acknowledges the following funding agencies for their support in building and running the ALICE detector: A. I. Alikhanyan National Science Laboratory (Yerevan Physics Institute) Foundation (ANSL), State Committee of Science and World Federation of Scientists (WFS), Armenia; Austrian Academy of Sciences, Austrian Science Fund (FWF): [M 2467-N36] and Nationalstiftung für Forschung, Technologie und Entwicklung, Austria; Ministry of Communications and High Technologies, National Nuclear Research Center, Azerbaijan; Rede Nacional de Física de Altas Energias (Renafae), Financiadora de Estudos e Projetos (Finep), Fundação de Amparo à Pesquisa do Estado de São Paulo (FAPESP) and The Sao Paulo Research Foundation (FAPESP), Brazil; Bulgarian Ministry of Education and Science, within the National Roadmap for Research Infrastructures 2020-2027 (object CERN), Bulgaria; Ministry of Education of China (MOEC), Ministry of Science & Technology of China (MSTC) and National Natural Science Foundation of China (NSFC), China; Ministry of Science and Education and Croatian Science Foundation, Croatia; Centro de Aplicaciones Tecnológicas y Desarrollo Nuclear (CEADEN), Cubaenergía, Cuba; Ministry of Education, Youth and Sports of the Czech Republic, Czech Republic; The Danish Council for Independent Research | Natural Sciences, the VILLUM FONDEN and Danish National Research Foundation (DNRF), Denmark; Helsinki Institute of Physics (HIP), Finland; Commissariat à l’Energie Atomique (CEA) and Institut National de Physique Nucléaire et de Physique des Particules (IN2P3) and Centre National de la Recherche Scientifique (CNRS), France; Bundesministerium für Forschung, Technologie und Raumfahrt (BMFTR) and GSI Helmholtzzentrum für Schwerionenforschung GmbH, Germany; National Research, Development and Innovation Office, Hungary; Department of Atomic Energy Government of India (DAE), Department of Science and Technology, Government of India (DST), University Grants Commission, Government of India (UGC) and Council of Scientific and Industrial Research (CSIR), India; National Research and Innovation Agency - BRIN, Indonesia; Istituto Nazionale di Fisica Nucleare (INFN), Italy; Japanese Ministry of Education, Culture, Sports, Science and Technology (MEXT) and Japan Society for the Promotion of Science (JSPS) KAKENHI, Japan; Consejo Nacional de Ciencia (CONACYT) y Tecnología, through Fondo de Cooperación Internacional en Ciencia y Tecnología (FONCICYT) and Dirección General de Asuntos del Personal Académico (DGAPA), Mexico; Nederlandse Organisatie voor Wetenschappelijk Onder-

zoek (NWO), Netherlands; The Research Council of Norway, Norway; Pontificia Universidad Católica del Perú, Peru; Ministry of Science and Higher Education, National Science Centre and WUT ID-UB, Poland; Korea Institute of Science and Technology Information and National Research Foundation of Korea (NRF), Republic of Korea; Ministry of Education and Scientific Research, Institute of Atomic Physics, Ministry of Research and Innovation and Institute of Atomic Physics and Universitatea Nationala de Stiinta si Tehnologie Politehnica Bucuresti, Romania; Ministerstvo skolstva, vyskumu, vyvoja a mladeze SR, Slovakia; National Research Foundation of South Africa, South Africa; Swedish Research Council (VR) and Knut & Alice Wallenberg Foundation (KAW), Sweden; European Organization for Nuclear Research, Switzerland; Suranaree University of Technology (SUT), National Science and Technology Development Agency (NSTDA) and National Science, Research and Innovation Fund (NSRF via PMU-B B05F650021), Thailand; Turkish Energy, Nuclear and Mineral Research Agency (TEN-MAK), Turkey; National Academy of Sciences of Ukraine, Ukraine; Science and Technology Facilities Council (STFC), United Kingdom; National Science Foundation of the United States of America (NSF) and United States Department of Energy, Office of Nuclear Physics (DOE NP), United States of America. In addition, individual groups or members have received support from: FORTE project, reg. no. CZ.02.01.01/00/22_008/0004632, Czech Republic, co-funded by the European Union, Czech Republic; European Research Council (grant no. 950692), European Union; Deutsche Forschungs Gemeinschaft (DFG, German Research Foundation) “Neutrinos and Dark Matter in Astro- and Particle Physics” (grant no. SFB 1258), Germany; FAIR - Future Artificial Intelligence Research, funded by the NextGenerationEU program (Italy).

References

- [1] **LHCb** Collaboration, R. Aaij *et al.*, “Measurement of forward J/ψ production cross-sections in pp collisions at $\sqrt{s} = 13$ TeV”, *JHEP* **10** (2015) 172, arXiv:1509.00771 [hep-ex]. [Erratum: *JHEP* 05, 063 (2017)].
- [2] **ALICE** Collaboration, S. Acharya *et al.*, “Energy dependence of forward-rapidity J/ψ and $\psi(2S)$ production in pp collisions at the LHC”, *Eur. Phys. J. C* **77** (2017) 392, arXiv:1702.00557 [hep-ex].
- [3] M. Butenschoen and B. A. Kniehl, “Probing nonrelativistic QCD factorization in polarized J/ψ photoproduction at next-to-leading order”, *Phys. Rev. Lett.* **107** (2011) 232001, arXiv:1109.1476 [hep-ph].
- [4] N. Brambilla *et al.*, “Heavy quarkonium: progress, puzzles, and opportunities”, *Eur. Phys. J. C* **71** (2011) 1534, arXiv:1010.5827 [hep-ph].
- [5] **ALICE** Collaboration, S. Acharya *et al.*, “Charm-quark fragmentation fractions and production cross section at midrapidity in pp collisions at the LHC”, *Phys. Rev. D* **105** (2022) L011103, arXiv:2105.06335 [nucl-ex].
- [6] **LHCb** Collaboration, R. Aaij *et al.*, “Enhanced production of Λ_b^0 baryons in high-multiplicity pp collisions at $\sqrt{s} = 13$ TeV”, *Phys. Rev. Lett.* **132** (2024) 081901, arXiv:2310.12278 [hep-ex].
- [7] C.-H. Chang, “Hadronic production of J/ψ associated with a gluon”, *Nucl. Phys. B* **172** (1980) 425–434.
- [8] R. Baier and R. Ruckl, “Hadronic production of J/ψ and Υ : transverse momentum distributions”, *Phys. Lett. B* **102** (1981) 364–370.
- [9] E. L. Berger and D. L. Jones, “Inelastic photoproduction of J/ψ and Υ by gluons”, *Phys. Rev. D* **23** (1981) 1521–1530.

- [10] M. B. Einhorn and S. D. Ellis, “Hadronic production of the new resonances: probing gluon distributions”, *Phys. Rev. D* **12** (1975) 2007.
- [11] C. E. Carlson and R. Suaya, “Hadronic production of J/ψ Mesons”, *Phys. Rev. D* **14** (1976) 3115.
- [12] J. P. Lansberg, “QCD corrections to J/ψ polarisation in pp collisions at RHIC”, *Phys. Lett. B* **695** (2011) 149–156, arXiv:1003.4319 [hep-ph].
- [13] CDF Collaboration, F. Abe *et al.*, “ J/ψ and $\psi(2S)$ production in $p\bar{p}$ collisions at $\sqrt{s} = 1.8$ TeV”, *Phys. Rev. Lett.* **79** (1997) 572–577.
- [14] ALICE Collaboration, B. B. Abelev *et al.*, “Measurement of quarkonium production at forward rapidity in pp collisions at $\sqrt{s} = 7$ TeV”, *Eur. Phys. J. C* **74** (2014) 2974, arXiv:1403.3648 [nucl-ex].
- [15] G. T. Bodwin, E. Braaten, and G. P. Lepage, “Rigorous QCD analysis of inclusive annihilation and production of heavy quarkonium”, *Phys. Rev. D* **51** (1995) 1125–1171, arXiv:hep-ph/9407339. [Erratum: Phys.Rev.D 55, 5853 (1997)].
- [16] Y.-Q. Ma, K. Wang, and K.-T. Chao, “A complete NLO calculation of the J/ψ and ψ' production at hadron colliders”, *Phys. Rev. D* **84** (2011) 114001, arXiv:1012.1030 [hep-ph].
- [17] M. Butenschoen and B. A. Kniehl, “Reconciling J/ψ production at HERA, RHIC, Tevatron, and LHC with NRQCD factorization at next-to-leading order”, *Phys. Rev. Lett.* **106** (2011) 022003, arXiv:1009.5662 [hep-ph].
- [18] G.-Z. Xu, Y.-J. Li, K.-Y. Liu, and Y.-J. Zhang, “Relativistic Correction to Color Octet J/ψ Production at Hadron Colliders”, *Phys. Rev. D* **86** (2012) 094017, arXiv:1203.0207 [hep-ph].
- [19] K.-T. Chao, Y.-Q. Ma, H.-S. Shao, K. Wang, and Y.-J. Zhang, “ J/ψ Polarization at Hadron Colliders in Nonrelativistic QCD”, *Phys. Rev. Lett.* **108** (2012) 242004, arXiv:1201.2675 [hep-ph].
- [20] M. Butenschoen and B. A. Kniehl, “ J/ψ polarization at Tevatron and LHC: Nonrelativistic-QCD factorization at the crossroads”, *Phys. Rev. Lett.* **108** (2012) 172002, arXiv:1201.1872 [hep-ph].
- [21] Y.-Q. Ma, T. Stebel, and R. Venugopalan, “ J/ψ polarization in the CGC+NRQCD approach”, *JHEP* **12** (2018) 057, arXiv:1809.03573 [hep-ph].
- [22] M. Butenschoen and B. A. Kniehl, “Global analysis of $\psi(2S)$ inclusive hadroproduction at next-to-leading order in nonrelativistic-QCD factorization”, *Phys. Rev. D* **107** (2023) 034003, arXiv:2207.09346 [hep-ph].
- [23] F. Halzen, “CVC for gluons and hadroproduction of quark flavors”, *Phys. Lett. B* **69** (1977) 105–108.
- [24] H. Fritzsche, “Producing heavy quark flavors in hadronic collisions: A test of quantum chromodynamics”, *Phys. Lett. B* **67** (1977) 217–221.
- [25] J. F. Amundson, O. J. P. Eboli, E. M. Gregores, and F. Halzen, “Quantitative tests of color evaporation: Charmonium production”, *Phys. Lett. B* **390** (1997) 323–328, arXiv:hep-ph/9605295.
- [26] Y.-Q. Ma and R. Vogt, “Quarkonium Production in an Improved Color Evaporation Model”, *Phys. Rev. D* **94** (2016) 114029, arXiv:1609.06042 [hep-ph].

- [27] S. Digal, P. Petreczky, and H. Satz, “Quarkonium feed down and sequential suppression”, *Phys. Rev. D* **64** (2001) 094015, arXiv:hep-ph/0106017.
- [28] J. Boyd, S. Thapa, and M. Strickland, “Transverse momentum dependent feed-down fractions for bottomonium production”, *Phys. Rev. D* **108** (2023) 094024, arXiv:2307.03841 [hep-ph].
- [29] G. Chen, X.-G. Wu, Z. Sun, X.-C. Zheng, and J.-M. Shen, “Next-to-leading order QCD corrections for the charmonium production via the channel $e^+e^- \rightarrow H(|c\bar{c}) + \gamma$ round the Z^0 peak”, *Phys. Rev. D* **89** (2014) 014006, arXiv:1311.2735 [hep-ph].
- [30] S. H. Lee and C. M. Ko, “Charmonium in nuclear matter”, *Phys. Rev. C* **67** (2003) 038202, arXiv:nucl-th/0208003.
- [31] A. Andronic and R. Arnaldi, “Quarkonia and Deconfined Quark–Gluon Matter in Heavy-Ion Collisions”, *Ann. Rev. Nucl. Part. Sci.* **75** (2025) 351–375, arXiv:2501.08290 [nucl-ex].
- [32] ALICE Collaboration, S. Acharya *et al.*, “Inclusive J/ψ production at midrapidity in pp collisions at $\sqrt{s} = 13$ TeV”, *Eur. Phys. J. C* **81** (2021) 1121, arXiv:2108.01906 [nucl-ex].
- [33] CMS Collaboration, A. M. Sirunyan *et al.*, “Measurement of quarkonium production cross sections in pp collisions at $\sqrt{s} = 13$ TeV”, *Phys. Lett. B* **780** (2018) 251–272, arXiv:1710.11002 [hep-ex].
- [34] ATLAS Collaboration, G. Aad *et al.*, “Measurement of the production cross-section of J/ψ and $\psi(2S)$ mesons in pp collisions at $\sqrt{s} = 13$ TeV with the ATLAS detector”, *Eur. Phys. J. C* **84** (2024) 169, arXiv:2309.17177 [hep-ex].
- [35] CMS Collaboration, S. Chatrchyan *et al.*, “ J/ψ and $\psi(2S)$ production in pp collisions at $\sqrt{s} = 7$ TeV”, *JHEP* **02** (2012) 011, arXiv:1111.1557 [hep-ex].
- [36] ATLAS Collaboration, M. Aaboud *et al.*, “Measurements of $\psi(2S)$ and $X(3872) \rightarrow J/\psi\pi^+\pi^-$ production in pp collisions at $\sqrt{s} = 8$ TeV with the ATLAS detector”, *JHEP* **01** (2017) 117, arXiv:1610.09303 [hep-ex].
- [37] CMS Collaboration, A. M. Sirunyan *et al.*, “Measurement of prompt $\psi(2S)$ production cross sections in proton-lead and proton-proton collisions at $\sqrt{s_{NN}} = 5.02$ TeV”, *Phys. Lett. B* **790** (2019) 509–532, arXiv:1805.02248 [hep-ex].
- [38] ALICE Collaboration, K. Aamodt *et al.*, “The ALICE experiment at the CERN LHC”, *JINST* **3** (2008) S08002.
- [39] ALICE Collaboration, B. B. Abelev *et al.*, “Performance of the ALICE Experiment at the CERN LHC”, *Int. J. Mod. Phys. A* **29** (2014) 1430044, arXiv:1402.4476 [nucl-ex].
- [40] ALICE Collaboration, K. Aamodt *et al.*, “Alignment of the ALICE Inner Tracking System with cosmic-ray tracks”, *JINST* **5** (2010) P03003, arXiv:1001.0502 [physics.ins-det].
- [41] J. Alme *et al.*, “The ALICE TPC, a large 3-dimensional tracking device with fast readout for ultra-high multiplicity events”, *Nucl. Instrum. Meth. A* **622** (2010) 316–367, arXiv:1001.1950 [physics.ins-det].
- [42] ALICE Collaboration, S. Acharya *et al.*, “The ALICE Transition Radiation Detector: construction, operation, and performance”, *Nucl. Instrum. Meth. A* **881** (2018) 88–127, arXiv:1709.02743 [physics.ins-det].

- [43] **ALICE** Collaboration, E. Abbas *et al.*, “Performance of the ALICE VZERO system”, *JINST* **8** (2013) P10016, arXiv:1306.3130 [nucl-ex].
- [44] **ALICE** Collaboration, S. Acharya *et al.*, “ J/ψ production at midrapidity in p–Pb collisions at $\sqrt{s_{NN}} = 8.16$ TeV”, *JHEP* **07** (2023) 137, arXiv:2211.14153 [nucl-ex].
- [45] S. van der Meer, “Calibration of the effective beam height in the ISR”, tech. rep., CERN, Geneva, 1968. <https://cds.cern.ch/record/296752>.
- [46] **ALICE** Collaboration, S. Acharya *et al.*, “ALICE 2016-2017-2018 luminosity determination for pp collisions at $\sqrt{s} = 13$ TeV”, 2021. <https://cds.cern.ch/record/2776672>.
- [47] **Particle Data Group** Collaboration, R. L. Workman and Others, “Review of Particle Physics”, *PTEP* **2022** (2022) 083C01.
- [48] T. Sjostrand, S. Mrenna, and P. Z. Skands, “PYTHIA 6.4 Physics and Manual”, *JHEP* **05** (2006) 026, arXiv:hep-ph/0603175.
- [49] D. J. Lange, “The EvtGen particle decay simulation package”, *Nucl. Instrum. Meth. A* **462** (2001) 152–155.
- [50] R. Brun, F. Carminati, and S. Giani, “GEANT Detector Description and Simulation Tool.” 1994. <https://cds.cern.ch/record/1082634>. W5013, W-5013, CERN-W5013, CERN-W-5013.
- [51] **ALICE** Collaboration, S. Acharya *et al.*, “Dielectron production in proton-proton collisions at $\sqrt{s} = 7$ TeV”, *JHEP* **09** (2018) 064, arXiv:1805.04391 [hep-ex].
- [52] **ALICE** Collaboration, S. Acharya *et al.*, “Inclusive J/ψ production at forward and backward rapidity in p-Pb collisions at $\sqrt{s_{NN}} = 8.16$ TeV”, *JHEP* **07** (2018) 160, arXiv:1805.04381 [nucl-ex].
- [53] **ALICE** Collaboration, S. Acharya *et al.*, “Dielectron and heavy-quark production in inelastic and high-multiplicity proton-proton collisions at $\sqrt{s} = 13$ TeV”, *Phys. Lett. B* **788** (2019) 505–518, arXiv:1805.04407 [hep-ex].
- [54] **ALICE** Collaboration, S. Acharya *et al.*, “Measurement of D-meson production at mid-rapidity in pp collisions at $\sqrt{s} = 7$ TeV”, *Eur. Phys. J. C* **77** (2017) 550, arXiv:1702.00766 [hep-ex].
- [55] G. Gatoff and C. Y. Wong, “Origin of the soft p_T spectra”, *Phys. Rev. D* **46** (1992) 997–1006.
- [56] G. D. Lafferty and T. R. Wyatt, “Where to stick your data points: The treatment of measurements within wide bins”, *Nucl. Instrum. Meth. A* **355** (1995) 541–547.
- [57] V. Cheung and R. Vogt, “Production and polarization of prompt J/ψ in the improved color evaporation model using the k_T -factorization approach”, *Phys. Rev. D* **98** (2018) 114029, arXiv:1808.02909 [hep-ph].
- [58] M. Cacciari, M. Greco, and P. Nason, “The p_T spectrum in heavy-flavour hadroproduction”, *JHEP* **05** (1998) 007, arXiv:hep-ph/9803400.
- [59] R. E. Nelson, R. Vogt, and A. D. Frawley, “Narrowing the uncertainty on the total charm cross section and its effect on the J/ψ cross section”, *Phys. Rev. C* **87** (2013) 014908, arXiv:1210.4610 [hep-ph].
- [60] **CDF** Collaboration, T. Aaltonen *et al.*, “Production of $\psi(2S)$ mesons in $p\bar{p}$ collisions at 1.96 TeV”, *Phys. Rev. D* **80** (2009) 031103, arXiv:0905.1982 [hep-ex].

A The ALICE Collaboration

D.A.H. Abdallah ¹³⁴, I.J. Abualrob ¹¹², S. Acharya ⁴⁹, K. Agarwal ^{II,23}, G. Aglieri Rinella ³², L. Aglietta ²⁴, N. Agrawal ²⁵, Z. Ahammed ¹³², S. Ahmad ¹⁵, I. Ahuja ³⁶, Z. Akbar ⁷⁹, V. Akishina ³⁸, M. Al-Turany ⁹⁴, B. Alessandro ⁵⁵, R. Alfaro Molina ⁶⁶, B. Ali ¹⁵, A. Alici ^{I,25}, J. Alme ²⁰, G. Alocco ²⁴, T. Alt ⁶³, I. Altsybeev ⁹², C. Andrei ⁴⁴, N. Andreou ¹¹¹, A. Andronic ¹²³, M. Angeletti ³², V. Anguelov ⁹¹, F. Antinori ⁵³, P. Antonioli ⁵⁰, N. Apadula ⁷¹, H. Appelshäuser ⁶³, S. Arcelli ^{I,25}, R. Arnaldi ⁵⁵, I.C. Arsene ¹⁹, M. Arslandok ¹³⁵, A. Augustinus ³², R. Averbeck ⁹⁴, M.D. Azmi ¹⁵, H. Baba ¹²¹, A.R.J. Babu ¹³⁴, A. Badalà ⁵², J. Bae ¹⁰⁰, Y. Bae ¹⁰⁰, Y.W. Baek ¹⁰⁰, X. Bai ¹¹⁶, R. Bailhache ⁶³, Y. Bailung ¹²⁵, R. Bala ⁸⁸, A. Baldisseri ¹²⁷, B. Balis ², S. Bangalia ¹¹⁴, Z. Banoo ⁸⁸, V. Barbasova ³⁶, F. Barile ³¹, L. Barioglio ⁵⁵, M. Barlou ²⁴, B. Barman ⁴⁰, G.G. Barnaföldi ⁴⁵, L.S. Barnby ¹¹¹, E. Barreau ⁹⁹, V. Barret ¹²⁴, L. Barreto ¹⁰⁶, K. Barth ³², E. Bartsch ⁶³, N. Bastid ¹²⁴, G. Batigne ⁹⁹, D. Battistini ^{34,92}, B. Batyunya ¹³⁹, L. Baudino ²⁴, D. Bauri ⁴⁶, J.L. Bazo Alba ⁹⁸, I.G. Bearden ⁸⁰, P. Becht ⁹⁴, D. Behera ^{77,47}, S. Behera ⁴⁶, I. Belikov ¹²⁶, V.D. Bella ¹²⁶, F. Bellini ²⁵, R. Bellwied ¹¹², L.G.E. Beltran ¹⁰⁵, Y.A.V. Beltran ⁴³, G. Bencedi ⁴⁵, O. Benchikhi ⁷³, A. Bensaoula ¹¹², S. Beole ²⁴, A. Berdnikova ⁹¹, L. Bergmann ⁷¹, L. Bernardinis ²³, L. Betev ³², P.P. Bhaduri ¹³², T. Bhalla ⁸⁷, A. Bhasin ⁸⁸, B. Bhattacharjee ⁴⁰, L. Bianchi ²⁴, J. Bielčik ³⁴, J. Bielčíková ⁸³, A. Bilandzic ⁹², A. Binoy ¹¹⁴, G. Biro ⁴⁵, S. Biswas ⁴, M.B. Blidaru ⁹⁴, N. Bluhme ³⁸, C. Blume ⁶³, F. Bock ⁸⁴, T. Bodova ²⁰, L. Boldizsár ⁴⁵, M. Bombara ³⁶, P.M. Bond ³², G. Bonomi ^{131,54}, H. Borel ¹²⁷, A. Borissov ¹³⁹, A.G. Borquez Carcamo ⁹¹, E. Botta ²⁴, N. Bouchhar ¹⁷, Y.E.M. Bouziani ⁶³, D.C. Brandibur ⁶², L. Bratrud ⁶³, P. Braun-Munzinger ⁹⁴, M. Bregant ¹⁰⁶, M. Broz ³⁴, G.E. Bruno ^{93,31}, V.D. Buchakchiev ³⁵, M.D. Buckland ⁸², H. Buesching ⁶³, S. Bufalino ²⁹, P. Buhler ⁷³, N. Burmasov ¹³⁹, Z. Buthelezi ^{67,120}, A. Bylinkin ²⁰, C. Carr ⁹⁷, J.C. Cabanillas Noris ¹⁰⁵, M.F.T. Cabrera ¹¹², H. Caines ¹³⁵, A. Caliva ²⁸, E. Calvo Villar ⁹⁸, J.M.M. Camacho ¹⁰⁵, P. Camerini ²³, M.T. Camerlingo ⁴⁹, F.D.M. Canedo ¹⁰⁶, S. Cannito ²³, S.L. Cantway ¹³⁵, M. Carabas ¹⁰⁹, F. Carnesecchi ³², L.A.D. Carvalho ¹⁰⁶, J. Castillo Castellanos ¹²⁷, M. Castoldi ³², F. Catalano ¹¹², S. Cattaruzzi ²³, R. Cerri ²⁴, I. Chakaberia ⁷¹, P. Chakraborty ¹³³, J.W.O. Chan ¹¹², S. Chandra ¹³², S. Chapeland ³², M. Chartier ¹¹⁵, S. Chattopadhyay ¹³², M. Chen ³⁹, T. Cheng ⁶, M.I. Cherciu ⁶², C. Cheshkov ¹²⁵, D. Chiappara ²⁷, V. Chibante Barroso ³², D.D. Chinellato ⁷³, F. Chinu ²⁴, E.S. Chizzali ^{III,92}, J. Cho ⁵⁷, S. Cho ⁵⁷, P. Chochula ³², Z.A. Chochulska ^{IV,133}, P. Christakoglou ⁸¹, P. Christiansen ⁷², T. Chujo ¹²², B. Chytla ¹³³, M. Ciacco ²⁴, C. Cicalo ⁵¹, G. Cimator ^{32,24}, F. Cindolo ⁵⁰, F. Colamaria ⁴⁹, D. Colella ³¹, A. Colelli ³¹, M. Colocci ²⁵, M. Concas ³², G. Conesa Balbastre ⁷⁰, Z. Conesa del Valle ¹²⁸, G. Contin ²³, J.G. Contreras ³⁴, M.L. Coquet ⁹⁹, P. Cortese ^{130,55}, M.R. Cosentino ¹⁰⁸, F. Costa ³², S. Costanza ²¹, P. Crochet ¹²⁴, M.M. Czarnynoga ¹³³, A. Dainese ⁵³, E. Dall'occo ³², G. Dange ³⁸, M.C. Danisch ¹⁶, A. Danu ⁶², A. Daribayeva ³⁸, P. Das ³², S. Das ⁴, A.R. Dash ¹²³, S. Dash ⁴⁶, A. De Caro ²⁸, G. de Cataldo ⁴⁹, J. de Cuveland ³⁸, A. De Falco ²², D. De Gruttola ²⁸, N. De Marco ⁵⁵, C. De Martin ²³, S. De Pasquale ²⁸, R. Deb ¹³¹, R. Del Grande ³⁴, L. Dello Stritto ³², G.G.A. de Souza ^{V,106}, P. Dhankeer ¹⁸, D. Di Bari ³¹, M. Di Costanzo ²⁹, A. Di Mauro ³², B. Di Ruzza ^{I,129,49}, B. Diab ³², Y. Ding ⁶, J. Ditzel ⁶³, R. Divià ³², U. Dmitrieva ⁵⁵, A. Dobrin ⁶², B. Dönigus ⁶³, L. Döpper ⁴¹, L. Drzensla ², J.M. Dubinski ¹³³, A. Dubla ⁹⁴, P. Dupieux ¹²⁴, N. Dzalaiiova ¹³, T.M. Eder ¹²³, R.J. Ehlers ⁷¹, F. Eisenhut ⁶³, R. Ejima ⁸⁹, D. Elia ⁴⁹, B. Erazmus ⁹⁹, F. Ercolessi ²⁵, B. Espagnon ¹²⁸, G. Eulisse ³², D. Evans ⁹⁷, L. Fabbietti ⁹², G. Fabbri ⁵⁰, M. Faggin ³², J. Faivre ⁷⁰, W. Fan ¹¹², T. Fang ⁶, A. Fantoni ⁴⁸, A. Feliciello ⁵⁵, W. Feng ⁶, A. Fernández Téllez ⁴³, B. Fernando ¹³⁴, L. Ferrandi ¹⁰⁶, A. Ferrero ¹²⁷, C. Ferrero ^{VI,55}, A. Ferretti ²⁴, D. Finogeev ¹³⁹, F.M. Fionda ⁵¹, A.N. Flores ¹⁰⁴, S. Foertsch ⁶⁷, I. Fokin ⁹¹, U. Follo ^{VI,55}, R. Forynski ¹¹¹, E. Fragiaco ⁵⁶, H. Fribert ⁹², U. Fuchs ³², D. Fuligno ²³, N. Funicello ²⁸, C. Furget ⁷⁰, A. Furs ¹³⁹, T. Fusayasu ⁹⁵, J.J. Gaardhøje ⁸⁰, M. Gagliardi ²⁴, A.M. Gago ⁹⁸, T. Gahlaut ⁴⁶, C.D. Galvan ¹⁰⁵, S. Gami ⁷⁷, C. Garabatos ⁹⁴, J.M. Garcia ⁴³, E. Garcia-Solis ⁹, S. Garetti ¹²⁸, C. Gargiulo ³², P. Gasik ⁹⁴, A. Gautam ¹¹⁴, M.B. Gay Ducati ⁶⁵, M. Germain ⁹⁹, R.A. Gernhaeuser ⁹², M. Giacalone ³², G. Gioachin ²⁹, S.K. Giri ¹³², P. Giubellino ⁵⁵, P. Giubileo ²⁷, P. Glässel ⁹¹, E. Glimos ¹¹⁹, M.G.F.S.A. Gomes ⁹¹, L. Gonella ²³, V. Gonzalez ¹³⁴, M. Gorgon ², K. Goswami ⁴⁷, S. Gotovac ³³, V. Grabski ⁶⁶, L.K. Graczykowski ¹³³, E. Grecka ⁸³, A. Grelli ⁵⁸, C. Grigoras ³², S. Grigoryan ^{139,1}, O.S. Groettvik ³², M. Gronbeck ⁴¹, F. Grosa ³², S. Gross-Böling ⁹⁴, J.F. Grosse-Oetringhaus ³², R. Grosso ⁹⁴, D. Grund ³⁴, N.A. Grunwald ⁹¹, R. Guernano ⁷⁰, M. Guilbaud ⁹⁹, K. Gulbrandsen ⁸⁰, J.K. Gumprecht ⁷³, T. Gündem ⁶³, T. Gunji ¹²¹, J. Guo ¹⁰, W. Guo ⁶, A. Gupta ⁸⁸, R. Gupta ⁸⁸, R. Gupta ⁴⁷, K. Gwizdz ¹³³, L. Gyulai ⁴⁵, T. Hachiya ⁷⁵, C. Hadjidakis ¹²⁸, F.U. Haider ⁸⁸,

S. Haidlova³⁴, M. Haldar⁴, W. Ham¹⁰⁰, H. Hamagaki⁷⁴, Y. Han¹³⁷, R. Hannigan¹⁰⁴, J. Hansen⁷², J.W. Harris¹³⁵, A. Harton⁹, M.V. Hartung⁶³, A. Hasan¹¹⁸, H. Hassan¹¹³, D. Hatzifotiadiou⁵⁰, P. Hauer⁴¹, L.B. Havener¹³⁵, E. Hellbär³², H. Helstrup³⁷, M. Hemmer⁶³, S.G. Hernandez¹¹², G. Herrera Corral⁸, K.F. Hetland³⁷, B. Heybeck⁶³, H. Hillemanns³², B. Hippolyte¹²⁶, I.P.M. Hobus⁸¹, F.W. Hoffmann³⁸, B. Hofman⁵⁸, Y. Hong⁵⁷, A. Horzyk², Y. Hou^{94,11}, P. Hristov³², L.M. Huhta¹¹³, T.J. Humanic⁸⁵, V. Humlova³⁴, M. Husar⁸⁶, A. Hutson¹¹², D. Hutter³⁸, M.C. Hwang¹⁸, M. Inaba¹²², A. Isakov⁸¹, T. Isidori¹¹⁴, M.S. Islam⁴⁶, M. Ivanov¹³, M. Ivanov⁹⁴, K.E. Iversen⁷², J.G. Kim¹³⁷, M. Jablonski², B. Jacak^{18,71}, N. Jacazio²⁵, P.M. Jacobs⁷¹, A. Jadlovska¹⁰², S. Jadlovska¹⁰², S. Jaelani⁷⁹, C. Jahnke¹⁰⁷, M.J. Jakubowska¹³³, E.P. Jamro², D.M. Janik³⁴, M.A. Janik¹³³, S. Ji¹⁶, Y. Ji⁹⁴, S. Jia⁸⁰, T. Jiang¹⁰, A.A.P. Jimenez⁶⁴, S. Jin¹⁰, F. Jonas⁷¹, D.M. Jones¹¹⁵, J.M. Jowett^{32,94}, J. Jung⁶³, M. Jung⁶³, A. Junique³², J. Juracka³⁴, J. Kaewjai^{115,101}, A. Kaiser^{32,94}, P. Kalinak⁵⁹, A. Kalweit³², A. Karasu Uysal¹³⁶, N. Karatzenis⁹⁷, T. Karavicheva¹³⁹, M.J. Karwowska¹³³, V. Kashyap⁷⁷, M. Keil³², B. Ketzer⁴¹, J. Keul⁶³, S.S. Khade⁴⁷, A. Khuntia⁵⁰, Z. Khuranova⁶³, B. Kileng³⁷, B. Kim¹⁰⁰, D.J. Kim¹¹³, D. Kim¹⁰⁰, E.J. Kim⁶⁸, G. Kim⁵⁷, H. Kim⁵⁷, J. Kim¹³⁷, J. Kim⁵⁷, J. Kim³², M. Kim¹⁸, S. Kim¹⁷, T. Kim¹³⁷, J.T. Kinner¹²³, I. Kisel³⁸, A. Kisiel¹³³, J.L. Klay⁵, J. Klein³², S. Klein⁷¹, C. Klein-Bösing¹²³, M. Kleiner⁶³, A. Kluge³², M.B. Knuesel¹³⁵, C. Kobdaj¹⁰¹, R. Kohara¹²¹, A. Kondratyev¹³⁹, J. Konig⁶³, P.J. Konopka³², G. Kornakov¹³³, M. Korwieser⁹², C. Koster⁸¹, A. Kotliarov⁸³, N. Kovacic⁸⁶, M. Kowalski¹⁰³, V. Kozhuharov³⁵, G. Kozlov³⁸, I. Králik⁵⁹, A. Kravčáková³⁶, M.A. Krawczyk³², L. Krcal³², F. Krizek⁸³, K. Krizkova Gajdosova³⁴, C. Krug⁶⁵, M. Krüger⁶³, E. Kryshen¹³⁹, V. Kučera⁵⁷, C. Kuhn¹²⁶, D. Kumar¹³², L. Kumar⁸⁷, N. Kumar⁸⁷, S. Kumar⁴⁹, S. Kundu³², M. Kuo¹²², P. Kurashvili⁷⁶, S. Kurita⁸⁹, S. Kushpil⁸³, A. Kuznetsov¹³⁹, M.J. Kweon⁵⁷, Y. Kwon¹³⁷, S.L. La Pointe³⁸, P. La Rocca²⁶, A. Lakrathok¹⁰¹, S. Lambert⁹⁹, A.R. Landou⁷⁰, R. Langoy¹¹⁸, P. Larionov³², E. Laudi³², L. Lautner⁹², R.A.N. Laveaga¹⁰⁵, R. Lavicka⁷³, R. Lea^{131,54}, J.B. Lebert³⁸, H. Lee¹⁰⁰, S. Lee⁵⁷, I. Legrand⁴⁴, G. Legras¹²³, A.M. Lejeune³⁴, T.M. Lelek², I. León Monzón¹⁰⁵, M.M. Lesch⁹², P. Lévai⁴⁵, M. Li⁶, P. Li¹⁰, X. Li¹⁰, B.E. Liang-Gilman¹⁸, J. Lien¹¹⁸, R. Lietava⁹⁷, I. Likmeta¹¹², B. Lim⁵⁵, H. Lim¹⁶, S.H. Lim¹⁶, Y.N. Lima¹⁰⁶, S. Lin¹⁰, V. Lindenstruth³⁸, C. Lippmann⁹⁴, D. Liskova¹⁰², D.H. Liu⁶, J. Liu¹¹⁵, Y. Liu⁶, G.S.S. Liveraro¹⁰⁷, I.M. Lofnes²⁰, C. Loizides²⁰, S. Lokos¹⁰³, J. Lömker⁵⁸, X. Lopez¹²⁴, E. López Torres⁷, C. Lotteau¹²⁵, P. Lu¹¹⁶, W. Lu⁶, Z. Lu¹⁰, O. Lubyets⁹⁴, G.A. Lucia²⁹, F.V. Lugo⁶⁶, J. Luo³⁹, G. Luparello⁵⁶, J. M. Friedrich⁹², Y.G. Ma³⁹, V. Machacek⁸⁰, M. Mager³², M. Mahlein⁹², A. Maire¹²⁶, E. Majerz², M.V. Makariev³⁵, G. Malfattore⁵⁰, N.M. Malik⁸⁸, N. Malik¹⁵, D. Mallick¹²⁸, N. Mallick¹¹³, G. Mandaglio^{30,52}, S. Mandal⁷⁷, S.K. Mandal⁷⁶, A. Manea⁶², R. Manhart⁹², A.K. Manna⁴⁷, F. Manso¹²⁴, G. Mantzaridis⁹², V. Manzari⁴⁹, Y. Mao⁶, R.W. Marcjan², G.V. Margagliotti²³, A. Margotti⁵⁰, A. Marín⁹⁴, C. Markert¹⁰⁴, P. Martinengo³², M.I. Martínez⁴³, M.P.P. Martins^{32,106}, S. Masciocchi⁹⁴, M. Masera²⁴, A. Masoni⁵¹, L. Massacrier¹²⁸, O. Massen⁵⁸, A. Mastroserio^{129,49}, L. Mattei^{24,124}, S. Mattiazzo²⁷, A. Matyja¹⁰³, J.L. Mayo¹⁰⁴, F. Mazzaschi³², M. Mazzilli³¹, Y. Melikyan⁴², M. Melo¹⁰⁶, A. Menchaca-Rocha⁶⁶, J.E.M. Mendez⁶⁴, E. Meninno⁷³, M.W. Menzel^{32,91}, M. Meres¹³, L. Micheletti⁵⁵, D. Mihai¹⁰⁹, D.L. Mihaylov⁹², A.U. Mikalsen²⁰, K. Mikhaylov¹³⁹, L. Millot⁷⁰, N. Minafra¹¹⁴, D. Miśkowiec⁹⁴, A. Modak⁵⁶, B. Mohanty⁷⁷, M. Mohisin Khan^{VII,15}, M.A. Molander⁴², M.M. Mondal⁷⁷, S. Monira¹³³, D.A. Moreira De Godoy¹²³, A. Morsch³², C. Moscatelli²³, T. Mrnjavac³², S. Mrozinski⁶³, V. Muccifora⁴⁸, S. Muhuri¹³², A. Mulliri²², M.G. Munhoz¹⁰⁶, R.H. Munzer⁶³, L. Musa³², J. Musinsky⁵⁹, J.W. Myrcha¹³³, B. Naik¹²⁰, A.I. Nambrath¹⁸, B.K. Nandi⁴⁶, R. Nania⁵⁰, E. Nappi⁴⁹, A.F. Nassirpour¹⁷, V. Nastase¹⁰⁹, A. Nath⁹¹, N.F. Nathanson⁸⁰, A. Neagu¹⁹, L. Nellen⁶⁴, R. Nepeivoda⁷², S. Nese¹⁹, N. Nicassio³¹, B.S. Nielsen⁸⁰, E.G. Nielsen⁸⁰, F. Noferini⁵⁰, S. Noh¹², P. Nomokonov¹³⁹, J. Norman¹¹⁵, N. Novitzky⁸⁴, J. Nystrand²⁰, M.R. Ockleton¹¹⁵, M. Ogino⁷⁴, J. Oh¹⁶, S. Oh¹⁷, A. Ohlson⁷², M. Oida⁸⁹, L.A.D. Oliveira^{I,107}, C. Oppedisano⁵⁵, A. Ortiz Velasquez⁶⁴, H. Osanai⁷⁴, J. Otwinowski¹⁰³, M. Oya⁸⁹, K. Oyama⁷⁴, S. Padhan^{131,46}, D. Pagano^{131,54}, V. Pagliarino⁵⁵, G. Paić⁶⁴, A. Palasciano^{93,49}, I. Panasenکو⁷², P. Panigrahi⁴⁶, C. Pantouvakis²⁷, H. Park¹²², J. Park¹²², S. Park¹⁰⁰, T.Y. Park¹³⁷, J.E. Parkkila¹³³, P.B. Pati⁸⁰, Y. Patley⁴⁶, R.N. Patra⁴⁹, J. Patter⁴⁷, B. Paul¹³², F. Pazdic⁹⁷, H. Pei⁶, T. Peitzmann⁵⁸, X. Peng^{53,11}, S. Perciballi²⁴, G.M. Perez⁷, M. Petrovici⁴⁴, S. Piano⁵⁶, M. Pikna¹³, P. Pillot⁹⁹, O. Pinazza^{50,32}, C. Pinto³², S. Pisano⁴⁸, M. Płoskoń⁷¹, A. Plachta¹³³, M. Planinic⁸⁶, D.K. Plociennik², S. Politano³², N. Poljak⁸⁶, A. Pop⁴⁴, S. Porteboeuf-Houssais¹²⁴, J.S. Potgieter¹¹⁰, I.Y. Pozos⁴³, K.K. Pradhan⁴⁷, S.K. Prasad⁴, S. Prasad⁴⁷, R. Preghenella⁵⁰,

F. Prino ⁵⁵, C.A. Pruneau ¹³⁴, M. Puccio ³², S. Pucillo ²⁸, S. Pulawski ¹¹⁷, L. Quaglia ²⁴,
A.M.K. Radhakrishnan ⁴⁷, S. Ragoni ¹⁴, A. Rai ¹³⁵, A. Rakotozafindrabe ¹²⁷, N. Ramasubramanian ¹²⁵,
L. Ramello ^{130,55}, C.O. Ramírez-Álvarez ⁴³, M. Rasa ²⁶, S.S. Räsänen ⁴², R. Rath ⁹⁴, M.P. Rauch ²⁰,
I. Ravasenga ³², M. Razza ²⁵, K.F. Read ^{84,119}, C. Reckziegel ¹⁰⁸, A.R. Redelbach ³⁸,
K. Redlich ^{VIII,76}, C.A. Reetz ⁹⁴, H.D. Regules-Medel ⁴³, A. Rehman ²⁰, F. Reidt ³²,
H.A. Reme-Ness ³⁷, K. Reygers ⁹¹, M. Richter ²⁰, A.A. Riedel ⁹², W. Riegler ³², A.G. Riffero ²⁴,
M. Rignanese ²⁷, C. Ripoli ²⁸, C. Ristea ⁶², M.V. Rodriguez ³², M. Rodríguez Cahuantzi ⁴³,
K. Røed ¹⁹, E. Rogochaya ¹³⁹, D. Rohr ³², D. Röhrich ²⁰, S. Rojas Torres ³⁴, P.S. Rokita ¹³³,
G. Romanenko ²⁵, F. Ronchetti ³², D. Rosales Herrera ⁴³, E.D. Rosas ⁶⁴, K. Roslon ¹³³, A. Rossi ⁵³,
A. Roy ⁴⁷, A. Roy ¹¹⁸, S. Roy ⁴⁶, N. Rubini ⁵⁰, O. Rubza ^{I,15}, J.A. Rudolph ⁸¹, D. Ruggiano ¹³³,
R. Rui ²³, P.G. Russek ², A. Rustamov ⁷⁸, A. Rybicki ¹⁰³, L.C.V. Ryder ¹¹⁴, G. Ryu ⁶⁹, J. Ryu ¹⁶,
W. Rzesza ⁹², B. Sabiu ⁵⁰, R. Sadek ⁷¹, S. Sadhu ⁴¹, A. Saha ³¹, S. Saha ⁷⁷, B. Sahoo ⁴⁷,
R. Sahoo ⁴⁷, D. Sahu ⁶⁴, P.K. Sahu ⁶⁰, J. Saini ¹³², S. Sakai ¹²², S. Sambyal ⁸⁸, D. Samitz ⁷³,
I. Sanna ³², D. Sarkar ⁸⁰, V. Sarritzu ²², V.M. Sarti ⁹², M.H.P. Sas ⁸¹, U. Savino ²⁴, S. Sawan ⁷⁷,
E. Scapparone ⁵⁰, J. Schambach ⁸⁴, H.S. Scheid ³², C. Schiaua ⁴⁴, R. Schicker ⁹¹, F. Schlepfer ^{32,91},
A. Schmah ⁹⁴, C. Schmidt ⁹⁴, M. Schmidt ⁹⁰, J. Schoengarth ⁶³, R. Schotter ⁷³, A. Schröter ³⁸,
J. Schukraft ³², K. Schweda ⁹⁴, G. Scioli ²⁵, E. Scomparin ⁵⁵, J.E. Seger ¹⁴, D. Sekihata ¹²¹,
M. Selina ⁸¹, I. Selyuzhenkov ⁹⁴, S. Senyukov ¹²⁶, J.J. Seo ⁹¹, L. Serkin ^{IX,64}, L. Šerkšnytė ³²,
A. Sevcenco ⁶², T.J. Shaba ⁶⁷, A. Shabetai ⁹⁹, R. Shahoyan ³², B. Sharma ⁸⁸, D. Sharma ⁴⁶,
H. Sharma ⁵³, M. Sharma ⁸⁸, S. Sharma ⁸⁸, T. Sharma ⁴⁰, U. Sharma ⁸⁸, O. Sheibani ¹³⁴, K. Shigaki ⁸⁹,
M. Shimomura ⁷⁵, Q. Shou ³⁹, S. Siddhanta ⁵¹, T. Siemiarz ⁷⁶, T.F. Silva ¹⁰⁶, W.D. Silva ¹⁰⁶,
D. Silvermyr ⁷², T. Simantathammakul ¹⁰¹, R. Simeonov ³⁵, B. Singh ⁴⁶, B. Singh ⁸⁸, B. Singh ⁹²,
K. Singh ⁴⁷, R. Singh ⁷⁷, R. Singh ⁵³, S. Singh ¹⁵, T. Sinha ⁹⁶, B. Sitar ¹³, M. Sitta ^{130,55},
T.B. Skaali ¹⁹, G. Skorodumovs ⁹¹, N. Smirnov ¹³⁵, K.L. Smith ¹⁶, R.J.M. Snellings ⁵⁸,
E.H. Solheim ¹⁹, S. Solokhin ⁸¹, C. Sonnabend ^{32,94}, J.M. Sonneveld ⁸¹, F. Soramel ²⁷,
A.B. Soto-Hernandez ⁸⁵, R. Spijkers ⁸¹, C. Sporleder ¹¹³, I. Sputowska ¹⁰³, J. Staa ⁷², J. Stachel ⁹¹,
L.L. Stahl ¹⁰⁶, I. Stan ⁶², A.G. Stejskal ¹¹⁴, T. Stellhorn ¹²³, S.F. Stiefelmaier ⁹¹, D. Stocco ⁹⁹,
I. Storehaug ¹⁹, N.J. Strangmann ⁶³, P. Stratmann ¹²³, S. Strazzi ²⁵, A. Sturniolo ^{115,30,52}, Y. Su ⁶,
A.A.P. Suaide ¹⁰⁶, C. Suire ¹²⁸, A. Suiu ¹⁰⁹, M. Sukhanov ¹³⁹, M. Suljic ³², V. Sumberia ⁸⁸,
S. Sumowidagdo ⁷⁹, P. Sun ¹⁰, N.B. Sundstrom ⁵⁸, L.H. Tabares ⁷, A. Tabikh ⁷⁰, S.F. Taghavi ⁹²,
J. Takahashi ¹⁰⁷, M.A. Talamantes Johnson ⁴³, G.J. Tambave ⁷⁷, Z. Tang ¹¹⁶, J. Tanwar ⁸⁷, J.D. Tapia
Takaki ¹¹⁴, N. Tapus ¹⁰⁹, L.A. Tarasovicova ³⁶, M.G. Tarzila ⁴⁴, A. Tauro ³², A. Tavira García ^{104,128},
G. Tejeda Muñoz ⁴³, L. Terlizzi ²⁴, C. Terrevoli ⁴⁹, D. Thakur ⁵⁵, S. Thakur ⁴, M. Thogersen ¹⁹,
D. Thomas ¹⁰⁴, A.M. Tiekoetter ¹²³, N. Tiltmann ^{32,123}, A.R. Timmins ¹¹², A. Toia ⁶³, R. Tokumoto ⁸⁹,
S. Tomassini ²⁵, K. Tomohiro ⁸⁹, Q. Tong ⁶, V.V. Torres ⁹⁹, A. Trifiró ^{30,52}, T. Triloki ⁹³, A.S. Triolo ³²,
S. Tripathy ³², T. Tripathy ¹²⁴, S. Trogolo ²⁴, V. Trubnikov ³, W.H. Trzaska ¹¹³, T.P. Trzcinski ¹³³,
C. Tsolanta ¹⁹, R. Tu ³⁹, R. Turrisi ⁵³, T.S. Tveter ¹⁹, K. Ullaland ²⁰, B. Ulukutlu ⁹², S. Upadhyaya ¹⁰³,
A. Uras ¹²⁵, M. Urioni ²³, G.L. Usai ²², M. Vaid ⁸⁸, M. Vala ³⁶, N. Valle ⁵⁴, L.V.R. van Doremalen ⁵⁸,
M. van Leeuwen ⁸¹, C.A. van Veen ⁹¹, R.J.G. van Weelden ⁸¹, D. Varga ⁴⁵, Z. Varga ¹³⁵,
P. Vargas Torres ⁶⁴, O. Vázquez Doce ⁴⁸, O. Vazquez Rueda ¹¹², G. Vecil ²³, P. Veen ¹²⁷,
E. Vercellin ²⁴, R. Verma ⁴⁶, R. Vértesi ⁴⁵, M. Verweij ⁵⁸, L. Vickovic ³³, Z. Vilakazi ¹²⁰, A. Villani ²³,
C.J.D. Villiers ⁶⁷, T. Virgili ²⁸, M.M.O. Virta ⁴², A. Vodopyanov ¹³⁹, M.A. Völkl ⁹⁷, S.A. Voloshin ¹³⁴,
G. Volpe ³¹, B. von Haller ³², I. Vorobyev ³², N. Vozniuk ¹³⁹, J. Vrláková ³⁶, J. Wan ³⁹, C. Wang ³⁹,
D. Wang ³⁹, Y. Wang ¹¹⁶, Y. Wang ³⁹, Y. Wang ⁶, Z. Wang ³⁹, F. Weiglhofer ³², S.C. Wenzel ³²,
J.P. Wessels ¹²³, P.K. Wiacek ², J. Wiechula ⁶³, J. Wikne ¹⁹, G. Wilk ⁷⁶, J. Wilkinson ⁹⁴,
G.A. Willems ¹²³, N. Wilson ¹¹⁵, B. Windelband ⁹¹, J. Witte ⁹¹, M. Wojnar ², C.I. Worek ²,
J.R. Wright ¹⁰⁴, C.-T. Wu ^{6,27}, W. Wu ^{92,39}, Y. Wu ¹¹⁶, K. Xiong ³⁹, Z. Xiong ¹¹⁶, L. Xu ^{125,6}, R. Xu ⁶,
Z. Xue ⁷¹, A. Yadav ⁴¹, A.K. Yadav ¹³², Y. Yamaguchi ⁸⁹, S. Yang ⁵⁷, S. Yang ²⁰, S. Yano ⁸⁹,
Z. Ye ⁷¹, E.R. Yeats ¹⁸, J. Yi ⁶, R. Yin ³⁹, Z. Yin ⁶, I.-K. Yoo ¹⁶, J.H. Yoon ⁵⁷, H. Yu ¹², S. Yuan ²⁰,
A. Yuncu ⁹¹, V. Zaccolo ²³, C. Zampolli ³², F. Zanone ⁹¹, N. Zardoshti ³², P. Závada ⁶¹, B. Zhang ⁹¹,
C. Zhang ¹²⁷, M. Zhang ^{124,6}, M. Zhang ^{27,6}, S. Zhang ³⁹, X. Zhang ⁶, Y. Zhang ¹¹⁶, Y. Zhang ¹¹⁶,
Z. Zhang ⁶, D. Zhou ⁶, Y. Zhou ⁸⁰, Z. Zhou ³⁹, J. Zhu ³⁹, S. Zhu ^{94,116}, Y. Zhu ⁶, A. Zingaretti ²⁷,
S.C. Zugravel ⁵⁵, N. Zurlo ^{131,54}

Affiliation Notes

- ^I Deceased
- ^{II} Also at: INFN Trieste
- ^{III} Also at: Max-Planck-Institut für Physik, Munich, Germany
- ^{IV} Also at: Czech Technical University in Prague (CZ)
- ^V Also at: Instituto de Física da Universidade de São Paulo
- ^{VI} Also at: Dipartimento DET del Politecnico di Torino, Turin, Italy
- ^{VII} Also at: Department of Applied Physics, Aligarh Muslim University, Aligarh, India
- ^{VIII} Also at: Institute of Theoretical Physics, University of Wrocław, Poland
- ^{IX} Also at: Facultad de Ciencias, Universidad Nacional Autónoma de México, Mexico City, Mexico

Collaboration Institutes

- ¹ A.I. Alikhanyan National Science Laboratory (Yerevan Physics Institute) Foundation, Yerevan, Armenia
- ² AGH University of Krakow, Cracow, Poland
- ³ Bogolyubov Institute for Theoretical Physics, National Academy of Sciences of Ukraine, Kyiv, Ukraine
- ⁴ Bose Institute, Department of Physics and Centre for Astroparticle Physics and Space Science (CAPSS), Kolkata, India
- ⁵ California Polytechnic State University, San Luis Obispo, California, United States
- ⁶ Central China Normal University, Wuhan, China
- ⁷ Centro de Aplicaciones Tecnológicas y Desarrollo Nuclear (CEADEN), Havana, Cuba
- ⁸ Centro de Investigación y de Estudios Avanzados (CINVESTAV), Mexico City and Mérida, Mexico
- ⁹ Chicago State University, Chicago, Illinois, United States
- ¹⁰ China Nuclear Data Center, China Institute of Atomic Energy, Beijing, China
- ¹¹ China University of Geosciences, Wuhan, China
- ¹² Chungbuk National University, Cheongju, Republic of Korea
- ¹³ Comenius University Bratislava, Faculty of Mathematics, Physics and Informatics, Bratislava, Slovak Republic
- ¹⁴ Creighton University, Omaha, Nebraska, United States
- ¹⁵ Department of Physics, Aligarh Muslim University, Aligarh, India
- ¹⁶ Department of Physics, Pusan National University, Pusan, Republic of Korea
- ¹⁷ Department of Physics, Sejong University, Seoul, Republic of Korea
- ¹⁸ Department of Physics, University of California, Berkeley, California, United States
- ¹⁹ Department of Physics, University of Oslo, Oslo, Norway
- ²⁰ Department of Physics and Technology, University of Bergen, Bergen, Norway
- ²¹ Dipartimento di Fisica, Università di Pavia, Pavia, Italy
- ²² Dipartimento di Fisica dell'Università and Sezione INFN, Cagliari, Italy
- ²³ Dipartimento di Fisica dell'Università and Sezione INFN, Trieste, Italy
- ²⁴ Dipartimento di Fisica dell'Università and Sezione INFN, Turin, Italy
- ²⁵ Dipartimento di Fisica e Astronomia dell'Università and Sezione INFN, Bologna, Italy
- ²⁶ Dipartimento di Fisica e Astronomia dell'Università and Sezione INFN, Catania, Italy
- ²⁷ Dipartimento di Fisica e Astronomia dell'Università and Sezione INFN, Padova, Italy
- ²⁸ Dipartimento di Fisica 'E.R. Caianiello' dell'Università and Gruppo Collegato INFN, Salerno, Italy
- ²⁹ Dipartimento DISAT del Politecnico and Sezione INFN, Turin, Italy
- ³⁰ Dipartimento di Scienze MIFT, Università di Messina, Messina, Italy
- ³¹ Dipartimento Interateneo di Fisica 'M. Merlin' and Sezione INFN, Bari, Italy
- ³² European Organization for Nuclear Research (CERN), Geneva, Switzerland
- ³³ Faculty of Electrical Engineering, Mechanical Engineering and Naval Architecture, University of Split, Split, Croatia
- ³⁴ Faculty of Nuclear Sciences and Physical Engineering, Czech Technical University in Prague, Prague, Czech Republic
- ³⁵ Faculty of Physics, Sofia University, Sofia, Bulgaria
- ³⁶ Faculty of Science, P.J. Šafárik University, Košice, Slovak Republic
- ³⁷ Faculty of Technology, Environmental and Social Sciences, Bergen, Norway
- ³⁸ Frankfurt Institute for Advanced Studies, Johann Wolfgang Goethe-Universität Frankfurt, Frankfurt, Germany
- ³⁹ Fudan University, Shanghai, China
- ⁴⁰ Gauhati University, Department of Physics, Guwahati, India

- 41 Helmholtz-Institut für Strahlen- und Kernphysik, Rheinische Friedrich-Wilhelms-Universität Bonn, Bonn, Germany
- 42 Helsinki Institute of Physics (HIP), Helsinki, Finland
- 43 High Energy Physics Group, Universidad Autónoma de Puebla, Puebla, Mexico
- 44 Horia Hulubei National Institute of Physics and Nuclear Engineering, Bucharest, Romania
- 45 HUN-REN Wigner Research Centre for Physics, Budapest, Hungary
- 46 Indian Institute of Technology Bombay (IIT), Mumbai, India
- 47 Indian Institute of Technology Indore, Indore, India
- 48 INFN, Laboratori Nazionali di Frascati, Frascati, Italy
- 49 INFN, Sezione di Bari, Bari, Italy
- 50 INFN, Sezione di Bologna, Bologna, Italy
- 51 INFN, Sezione di Cagliari, Cagliari, Italy
- 52 INFN, Sezione di Catania, Catania, Italy
- 53 INFN, Sezione di Padova, Padova, Italy
- 54 INFN, Sezione di Pavia, Pavia, Italy
- 55 INFN, Sezione di Torino, Turin, Italy
- 56 INFN, Sezione di Trieste, Trieste, Italy
- 57 Inha University, Incheon, Republic of Korea
- 58 Institute for Gravitational and Subatomic Physics (GRASP), Utrecht University/Nikhef, Utrecht, Netherlands
- 59 Institute of Experimental Physics, Slovak Academy of Sciences, Košice, Slovak Republic
- 60 Institute of Physics, Homi Bhabha National Institute, Bhubaneswar, India
- 61 Institute of Physics of the Czech Academy of Sciences, Prague, Czech Republic
- 62 Institute of Space Science (ISS), Bucharest, Romania
- 63 Institut für Kernphysik, Johann Wolfgang Goethe-Universität Frankfurt, Frankfurt, Germany
- 64 Instituto de Ciencias Nucleares, Universidad Nacional Autónoma de México, Mexico City, Mexico
- 65 Instituto de Física, Universidade Federal do Rio Grande do Sul (UFRGS), Porto Alegre, Brazil
- 66 Instituto de Física, Universidad Nacional Autónoma de México, Mexico City, Mexico
- 67 iThemba LABS, National Research Foundation, Somerset West, South Africa
- 68 Jeonbuk National University, Jeonju, Republic of Korea
- 69 Korea Institute of Science and Technology Information, Daejeon, Republic of Korea
- 70 Laboratoire de Physique Subatomique et de Cosmologie, Université Grenoble-Alpes, CNRS-IN2P3, Grenoble, France
- 71 Lawrence Berkeley National Laboratory, Berkeley, California, United States
- 72 Lund University Department of Physics, Division of Particle Physics, Lund, Sweden
- 73 Marietta Blau Institute, Vienna, Austria
- 74 Nagasaki Institute of Applied Science, Nagasaki, Japan
- 75 Nara Women's University (NWU), Nara, Japan
- 76 National Centre for Nuclear Research, Warsaw, Poland
- 77 National Institute of Science Education and Research, Homi Bhabha National Institute, Jatni, India
- 78 National Nuclear Research Center, Baku, Azerbaijan
- 79 National Research and Innovation Agency - BRIN, Jakarta, Indonesia
- 80 Niels Bohr Institute, University of Copenhagen, Copenhagen, Denmark
- 81 Nikhef, National institute for subatomic physics, Amsterdam, Netherlands
- 82 Nuclear Physics Group, STFC Daresbury Laboratory, Daresbury, United Kingdom
- 83 Nuclear Physics Institute of the Czech Academy of Sciences, Husinec-Řež, Czech Republic
- 84 Oak Ridge National Laboratory, Oak Ridge, Tennessee, United States
- 85 Ohio State University, Columbus, Ohio, United States
- 86 Physics department, Faculty of science, University of Zagreb, Zagreb, Croatia
- 87 Physics Department, Panjab University, Chandigarh, India
- 88 Physics Department, University of Jammu, Jammu, India
- 89 Physics Program and International Institute for Sustainability with Knotted Chiral Meta Matter (WPI-SKCM²), Hiroshima University, Hiroshima, Japan
- 90 Physikalisches Institut, Eberhard-Karls-Universität Tübingen, Tübingen, Germany
- 91 Physikalisches Institut, Ruprecht-Karls-Universität Heidelberg, Heidelberg, Germany
- 92 Physik Department, Technische Universität München, Munich, Germany
- 93 Politecnico di Bari and Sezione INFN, Bari, Italy

- ⁹⁴ Research Division and ExtreMe Matter Institute EMMI, GSI Helmholtzzentrum für Schwerionenforschung GmbH, Darmstadt, Germany
- ⁹⁵ Saga University, Saga, Japan
- ⁹⁶ Saha Institute of Nuclear Physics, Homi Bhabha National Institute, Kolkata, India
- ⁹⁷ School of Physics and Astronomy, University of Birmingham, Birmingham, United Kingdom
- ⁹⁸ Sección Física, Departamento de Ciencias, Pontificia Universidad Católica del Perú, Lima, Peru
- ⁹⁹ SUBATECH, IMT Atlantique, Nantes Université, CNRS-IN2P3, Nantes, France
- ¹⁰⁰ Sungkyunkwan University, Suwon City, Republic of Korea
- ¹⁰¹ Suranaree University of Technology, Nakhon Ratchasima, Thailand
- ¹⁰² Technical University of Košice, Košice, Slovak Republic
- ¹⁰³ The Henryk Niewodniczanski Institute of Nuclear Physics, Polish Academy of Sciences, Cracow, Poland
- ¹⁰⁴ The University of Texas at Austin, Austin, Texas, United States
- ¹⁰⁵ Universidad Autónoma de Sinaloa, Culiacán, Mexico
- ¹⁰⁶ Universidade de São Paulo (USP), São Paulo, Brazil
- ¹⁰⁷ Universidade Estadual de Campinas (UNICAMP), Campinas, Brazil
- ¹⁰⁸ Universidade Federal do ABC, Santo Andre, Brazil
- ¹⁰⁹ Universitatea Nationala de Stiinta si Tehnologie Politehnica Bucuresti, Bucharest, Romania
- ¹¹⁰ University of Cape Town, Cape Town, South Africa
- ¹¹¹ University of Derby, Derby, United Kingdom
- ¹¹² University of Houston, Houston, Texas, United States
- ¹¹³ University of Jyväskylä, Jyväskylä, Finland
- ¹¹⁴ University of Kansas, Lawrence, Kansas, United States
- ¹¹⁵ University of Liverpool, Liverpool, United Kingdom
- ¹¹⁶ University of Science and Technology of China, Hefei, China
- ¹¹⁷ University of Silesia in Katowice, Katowice, Poland
- ¹¹⁸ University of South-Eastern Norway, Kongsberg, Norway
- ¹¹⁹ University of Tennessee, Knoxville, Tennessee, United States
- ¹²⁰ University of the Witwatersrand, Johannesburg, South Africa
- ¹²¹ University of Tokyo, Tokyo, Japan
- ¹²² University of Tsukuba, Tsukuba, Japan
- ¹²³ Universität Münster, Institut für Kernphysik, Münster, Germany
- ¹²⁴ Université Clermont Auvergne, CNRS/IN2P3, LPC, Clermont-Ferrand, France
- ¹²⁵ Université de Lyon, CNRS/IN2P3, Institut de Physique des 2 Infinis de Lyon, Lyon, France
- ¹²⁶ Université de Strasbourg, CNRS, IPHC UMR 7178, F-67000 Strasbourg, France, Strasbourg, France
- ¹²⁷ Université Paris-Saclay, Centre d'Etudes de Saclay (CEA), IRFU, Département de Physique Nucléaire (DPhN), Saclay, France
- ¹²⁸ Université Paris-Saclay, CNRS/IN2P3, IJCLab, Orsay, France
- ¹²⁹ Università degli Studi di Foggia, Foggia, Italy
- ¹³⁰ Università del Piemonte Orientale, Vercelli, Italy
- ¹³¹ Università di Brescia, Brescia, Italy
- ¹³² Variable Energy Cyclotron Centre, Homi Bhabha National Institute, Kolkata, India
- ¹³³ Warsaw University of Technology, Warsaw, Poland
- ¹³⁴ Wayne State University, Detroit, Michigan, United States
- ¹³⁵ Yale University, New Haven, Connecticut, United States
- ¹³⁶ Yildiz Technical University, Istanbul, Turkey
- ¹³⁷ Yonsei University, Seoul, Republic of Korea
- ¹³⁸ Affiliated with an institute formerly covered by a cooperation agreement with CERN
- ¹³⁹ Affiliated with an international laboratory covered by a cooperation agreement with CERN.